ACS NANOSCIENCE Au
AN OPEN ACCESS JOURNAL OF THE AMERICAN CHEMICAL SOCIETY

pubs.acs.org/nanoau Review

Sonophotocatalysis with Photoactive Nanomaterials for Wastewater Treatment and Bacteria Disinfection

Sina Moradi, Cristina Rodriguez-Seco,* Farzan Hayati, and Dongling Ma*

Cite This: *ACS Nanosci. Au* 2023, 3, 103−129 Read Online

ACCESS | Metrics & More | Article Recommendations

ABSTRACT: Sonophotocatalysis is described as a combination of two individual processes of photocatalysis and sonocatalysis. It has proven to be highly promising in degrading dissolved contaminants in wastewaters as well as bacteria disinfection applications. It eliminates some of the main disadvantages observed in each individual technique such as high costs, sluggish activity, and prolonged reaction times. The review has accomplished a critical analysis of sonophotocatalytic reaction mechanisms and the effect of the nanostructured catalyst and process modification techniques on the sonophotocatalytic performance. The synergistic effect between the mentioned processes, reactor design, and the electrical energy consumption has been discussed due to their importance when implementing this novel technology in practical applications, such as real industrial or municipal wastewater treatment plants. The utilization of sonophotocatalysis in disinfection and inactivation of bacteria has also been reviewed. In addition, we further suggest improvements to promote this technology from the lab-scale to large-scale applications. We hope this up-to-date review will advance future research in this field and push this technology toward widespread adoption and commercialization.

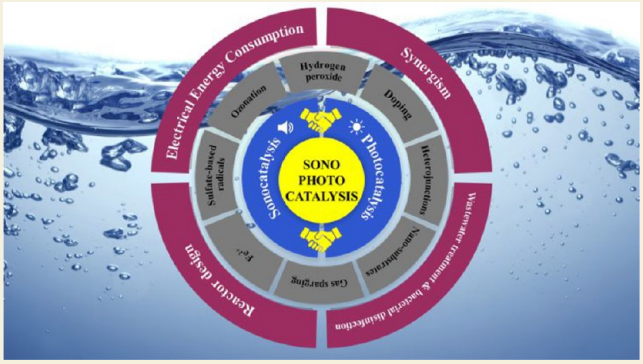

KEYWORDS: *sonophotocatalysis, nanomaterials, degradation, wastewater treatment, cavitation bubbles, sonoluminescence, sonophotocatalytic mechanisms, bacteria disinfection*

1. INTRODUCTION

Nowadays, water bodies are being contaminated by a broad range of pollutants at a sky-rocketing pace. Although there is no precise information associated with the amount of wastewater discharged to the environment, the horrible consequences of pollutants existing in the aquatic media have led to great public concerns (i.e., human and animal infections, and destruction of the natural habitats and the wildlife living in those territories).[1,2] There is an array of wastewater treatment approaches that have already been investigated, including biological, physical, and chemical treatments. Despite their cost-effectiveness, conventional methods still suffer from several shortcomings, such as being time-consuming, high cost of waste disposal, forming large amounts of slug, and too much sensitivity of living organisms to operational parameters.[3]

Over the past few decades, photocatalysis has been eliciting considerable interest for several reasons including low-cost, outstanding reusability and recyclability of photocatalysts, its ability to produce a high content of active radicals, negligible sludge generation, and high mineralization rate.[4] The photocatalysis process starts through the excitation of electrons and generation of holes in a semiconductor material (such as ZnS,[5] g-C_3N_4,[6] TiO_2,[7] ZnO,[8] CuO[9]) under the irradiation of a light source. However, the practical applications of conventional photocatalysts have been restricted due to some bottlenecks such as low efficiency, high recombination rate of electron/hole (e^-/h^+) pairs, and agglomeration of nanoparticle catalysts.[10] To overcome these hindrances, the combination of photocatalysis process with other methods, electrochemical and sonolysis techniques, has been proposed.

Sonochemistry refers to the chemical process realized by passing ultrasonic waves through liquid environments. It has been utilized for the degradation of several pollutants.[11,12] Coupling ultrasonic waves of specific frequencies (20−1000 kHz) with photocatalysis is postulated to be one of the most promising techniques for developing complete mineralization of recalcitrant contaminants since it improves the overall contaminant removal efficiency. Figure 1 depicts the growth in

Received: November 29, 2022
Revised: January 6, 2023
Accepted: January 9, 2023
Published: January 27, 2023

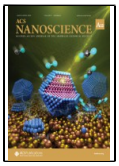

https://doi.org/10.1021/acsnanoscienceau.2c00058
ACS Nanosci. Au 2023, 3, 103−129

use of sonocatalysts, sonophotocatalysts, and sonophotocatalyst nanomaterials for wastewater treatment in the recent years.

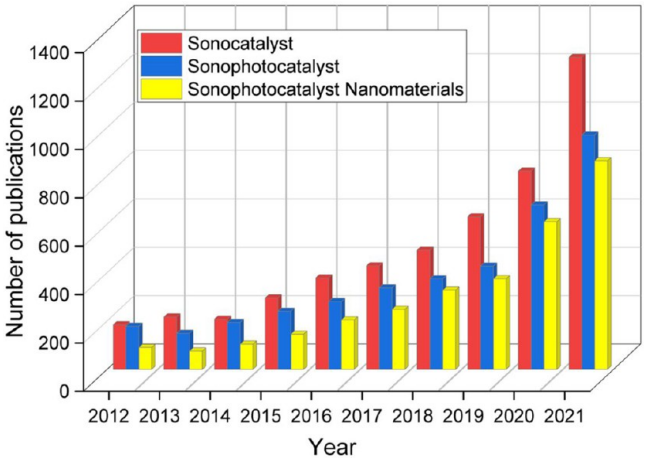

Figure 1. Number of publications searched with the words "Sonocatalyst", "Sonophotocatalyst", and "Sonophotocatalyst Nanomaterials" (Data obtained from *Google Scholar* on Nov 21, 2022).

Acoustic cavitation generated by powerful ultrasonic waves of a liquid can provide unique and unusual reaction sites. This is attributed to extremely small and transient cavitation microbubbles with high pressure and temperature (5000 K, 1000 atm) inside the bubble. Among all the advantages this process can provide, the most critical one is the unique release of an avalanche of reactive radicals, e.g., $OH^{\bullet}$ and $H^{\bullet}$, owing to the homolytic cleavage of water molecules.[13] These specific physical and chemical events generated during the cavitation process are often different from those taking place in traditional photochemical reactions. Providing large numbers of hot vapor sites in solution (microbubbles), ultrasonication expels hydrophobic pollutants to the liquid−vapor boundaries where they will be degraded effectively by either produced shock waves or radicals on-site, whereas hydrophilic contaminants can be removed by photocatalysis in liquid.[14] Therefore, both hydrophobic and hydrophilic contaminants can be effectively degraded in water, which is clearly advantageous over the traditional photocatalysis. Moreover, ultrasonication offers several additional benefits, like simple and safe operation and the formation of a large number of hydroxyl radicals ($OH^{\bullet}$) through different mechanisms.[15] Studies of the combination of light with ultrasound (US) irradiation for the removal of organics from wastewater have been reported, and the combined process was found to be significantly more effective than either process separately, showing a great synergistic enhancement effect.[16−20] This association provides an excellent opportunity to decrease the reaction time and the amount of photocatalyst utilized without using extreme physical conditions.

Recently, photocatalysis has been employed for the disinfection of pathogenic bacteria due to its potential to produce reactive oxygen species. It is true that photocatalysis is capable of deactivating water borne enteric bacteria, but there is a number of challenges associated with its implementation,[21,22] for example, prolonged exposure times, reactivation of bacteria after a photocatalytic process due to DNA repair mechanisms, and a decrease in active surface area because of agglomeration of photocatalysts.[23−25] Sonophotocatalysis—a hybrid disinfection strategy—is proposed as a solution to overcome these limitations of traditional photocatalysis.

Although there are a few review articles in this field, they do not include information related to reaction mechanisms in sonophotocatalysis. In this critical review, mainly focused on metal-oxide nanomaterials, we conducted a thorough analysis of ultrasonic-assisted photocatalytic mechanisms in wastewater treatment, their synergistic effects, and enhancing techniques. For the first time, an electrical energy consumption analysis has been performed, which allowed us to make a comparison between sonophotocatalysis, traditional photocatalysis, and sonocatalysis. In addition to the description of different reactor designs, we reviewed the application of sonophotocatalysis in bacterial disinfection. We hope this review article will contribute to the ongoing research into whether sonophotocatalysis could replace conventional photocatalysis or be used in large-scale wastewater treatment applications.

2. SONOPHOTOCATALYSIS MECHANISMS

As the name implies, sonophotocatalytic mechanisms include those of photocatalysis and sonocatalysis. Detailed explanations of each individual process will follow in order to explain the mechanisms clearly.

2.1. Photocatalysis Mechanisms

In order to highlight the differences between sonophotocatalysis and photocatalysis, we will first briefly describe the mechanism of traditional photocatalysis. Photocatalytic processes initiate with the exposure of catalytic semiconductor materials to a light source. In this step, photonic energy leads to the excitation of electrons from the valence band (VB) to conduction band (CB), creating positive holes in the VB. The reaction of oxygen molecules and hydrogen peroxide molecules (produced either *in situ* or intentionally introduced) with photoinduced electrons produces superoxide anion radicals ($O_2^{\bullet -}$) and $OH^{\bullet}$ radicals, respectively. Meanwhile, the reaction of water molecules with positive holes produces $OH^{\bullet}$ radical species (eqs 1−9).[10] These photoactivated systems have the ability to degrade a wide variety of pollutants (e.g., dyes and pharmaceuticals) and completely mineralize contaminants. On the other hand, these systems suffer from a few disadvantages, such as low reaction rate constants, low visible (Vis) light absorption of catalytic materials, and performance reduction over time due to catalytic particle agglomeration. These drawbacks restrict their utilization at an industrial scale.[26,27]

$$\text{catalyst} \xrightarrow{h\nu} h_{VB}^{+} + e_{CB}^{-} \quad (1)$$

$$H_2O + h^{+} \rightarrow H^{+} + OH^{\bullet} \quad (2)$$

$$O_2 + e^{-} \rightarrow O_2^{\bullet -} \quad (3)$$

$$O_2^{\bullet -} + H^{+} \rightarrow OOH^{\bullet} \quad (4)$$

$$2OH^{\bullet} \rightarrow H_2O_2 \quad (5)$$

$$H_2O_2 + e^{-} \rightarrow OH^{-} + OH^{\bullet}_{ads} \quad (6)$$

$$2OOH^{\bullet} \rightarrow H_2O_2 + O_2 \quad (7)$$

$$H^{\bullet} + H_2O_2 \rightarrow OH^{\bullet} + H_2O \quad (8)$$

$$OH^{\bullet} + H_2O_2 \rightarrow OOH^{\bullet} + H_2O \quad (9)$$

https://doi.org/10.1021/acsnanoscienceau.2c00058
ACS Nanosci. Au 2023, 3, 103−129

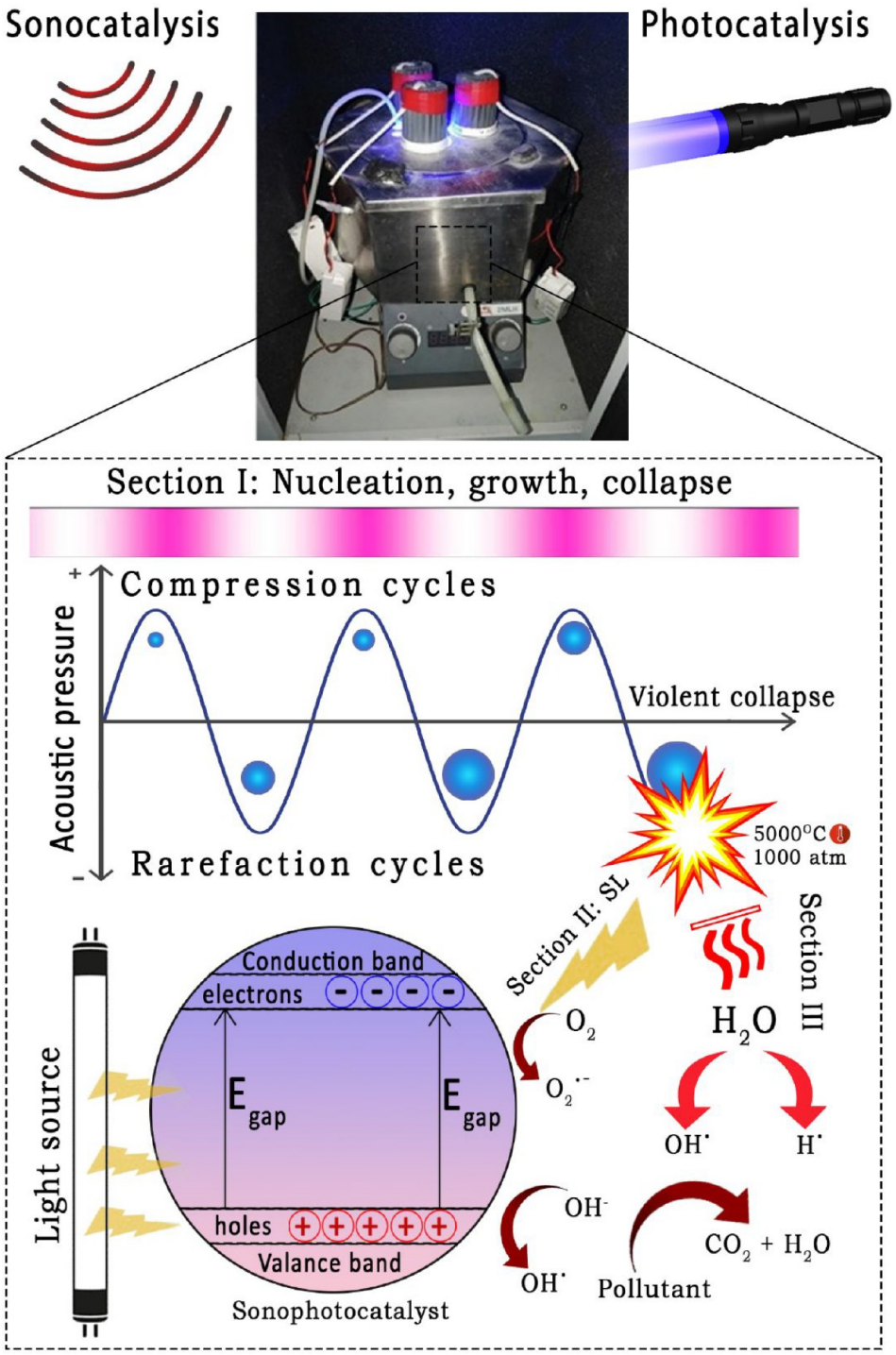

Figure 2. Illustration of sonophotocatalytic setup and degradation mechanism. The sonophotochemical reactor figure is reproduced with permission from ref 28. Copyright 2020 Elsevier.

2.2. Sonocatalysis Mechanisms

Among all the strategies adopted to overcome the photocatalysis shortcomings, integration with ultrasonic waves ranks top in terms of feasibility and effectiveness. The sonocatalysis mechanism consists in three key processes (see Section 1 in Figure 2).

First, at the phase boundary or solid surface, solid catalytic particles serve as additional nucleation sites for the heterogeneous nucleation of cavitation bubbles. It is notable that this process is different from homogeneous nucleation that occurs in the bulk solution by thermal fluctuations. Accordingly, cavitation bubbles are formed when acoustic cavitations reach rarefaction cycles (expansion) where an acoustic pressure is sufficiently high to dissociate water molecules. Having grown to an unstable and critical size during the rarefaction cycles, bubbles filled with vapor from the liquid and with dissolved gases can collapse violently, creating implosions and cavitations especially for high acoustic pressure amplitudes more than 1 bar.[29,30]

https://doi.org/10.1021/acsnanoscienceau.2c00058
ACS Nanosci. Au 2023, 3, 103−129

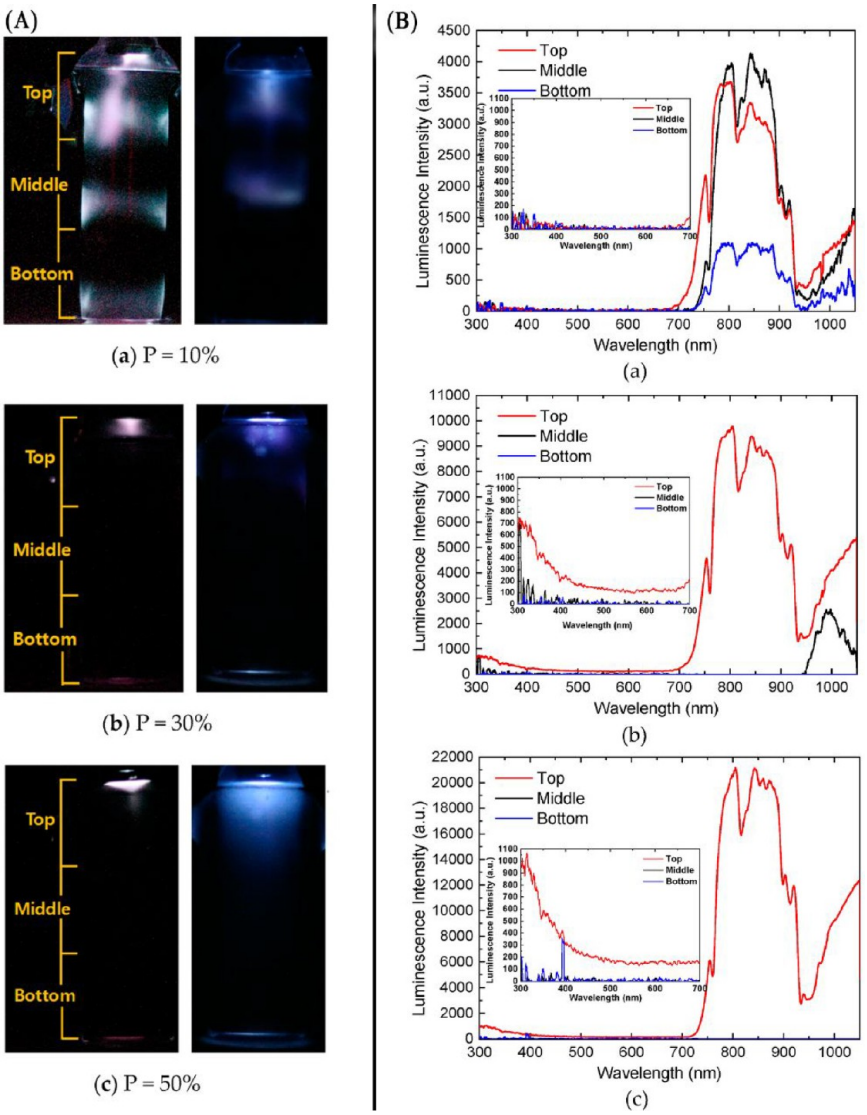

Figure 3. (A) Photographic images of SL (left images) and chemiluminescence (right images) in water at various US powers of (a) 10, (b) 30, and (c) 50%. (B) PL spectra of SL detected at three different zones of US reactor (red line, top; black line, middle; and blue line, bottom) with US power of (a) 10, (b) 30, and (c) 50%. Inset spectra are UV to Vis light range only. Reprinted with permission under a Creative Commons CC-BY license from ref 36. Copyright 2020 MDPI.

Sonoluminescence (SL) refers to emission of light by the collapse of cavitation bubbles. The second key step involves the collapse of cavitation bubbles, which results in SL, i.e., emission of light ranging from 200 nm to near-infrared (NIR) zone (longer than 700 nm) with relatively high intensity. This phenomenon happens only if the plasma energy is high enough to generate electronically excited species (ions, molecules radicals, etc.). Obviously, the energy threshold for excited species production during the bubble collapse is much higher than that for radical formation.[31] In this way, since the light energy from SL is greater than that of the semiconductor band gap, it could induce extra e^-/h^+ pairs, which leads to high reactive species production (eqs 1−4). Previous studies indicated that the excitation of TiO_2 catalyst by SL caused a remarkable decomposition of pollutants, such as methylene blue (MB) and phenol and 2,4-dinitrophenol, just as observed in photocatalytic processes.[32,33] The spectral shapes and intensities of SL rely on several parameters, such as the presence of additives, types of saturated gas, and the frequency and power of US.[31,34] For example, Qui et al.[35] calculated the SL power at a wavelength of 400 nm during sonocatalysis (energy 4.9×10^{-19} J). Since each flash of SL can last for about 50 ps, emitting approximately 10^7 photons, the power of SL for each second was 0.098 W. Choi et al.[36] detected the ultrasonic-induced SL through the sonophotocatalytic degradation of eosin B using commercial TiO_2, by means of photographic imaging, a radical indicator (luminol, $C_8H_6N_3O_2Na$) for detecting radical formation zones, and photoluminescence (PL) spectroscopy for detecting emitted photons in the wavelength range 300−1050 nm. At an US power of 35.4 W/cm^2, SL was observed in a standing wave pattern throughout the sonophotocatalytic reactor (Figure 3A). By increasing US intensity, this pattern disappeared and the SL mostly occurred at the ultrasonic horn tip. Authors highlighted that SL occurred mostly in the NIR range, and its intensity increased almost linearly with the US power (Figure 3B). PL measurements revealed that UV irradiations appear only when enough energy input was applied (106.1 and 176.8 W/cm^2). With the 35.4 W/cm^2 US intensity, band-type chemiluminescence arose at

https://doi.org/10.1021/acsnanoscienceau.2c00058
ACS Nanosci. Au 2023, 3, 103−129

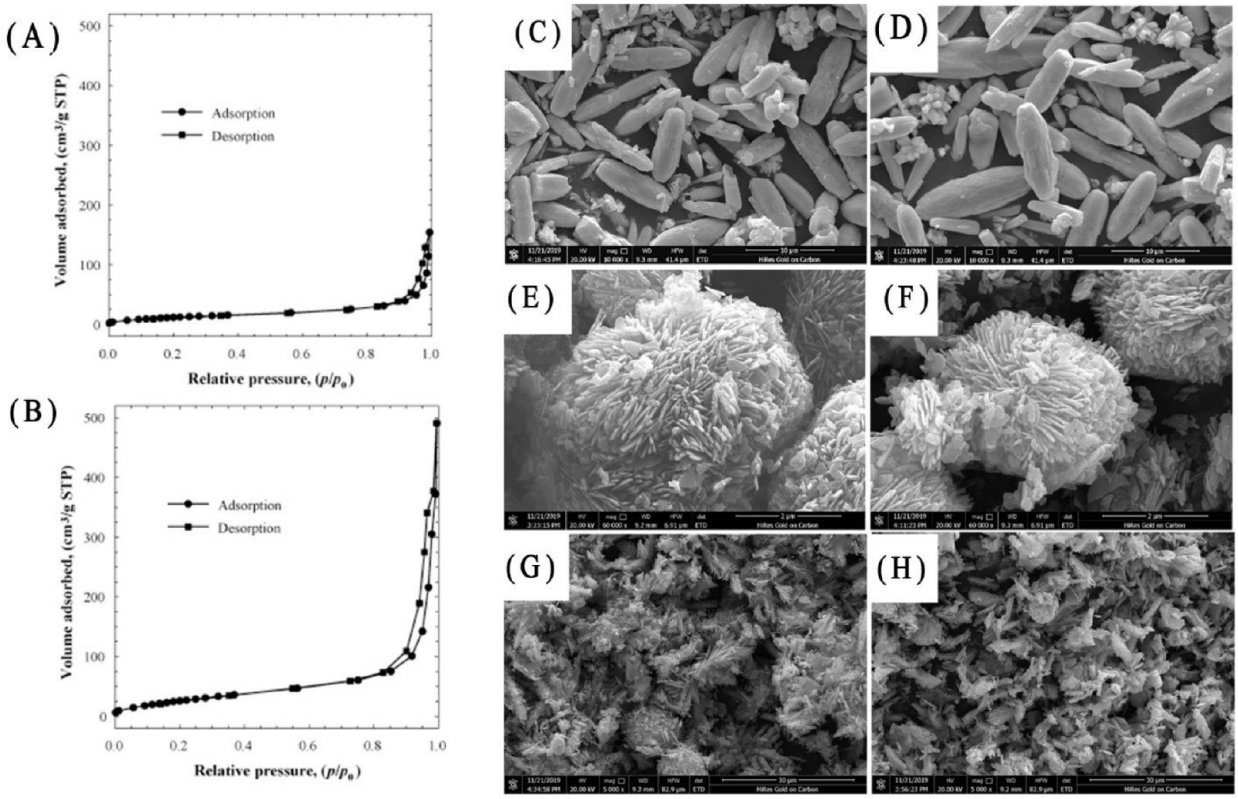

Figure 4. Adsorption/desorption isotherms of TiO_2 (A) before and (B) after H_2O_2-assisted sonophotocatalysis (model solution contained 13 compounds commonly found in olive mill wastewaters at the concentration of 50 mg/L each, UVA power of 400 W, and US power of 120 W at 80 kHz). SEM images of as-prepared ZnO samples before (C, E, and G) and after sonophotocatalysis (D, F, and H). (C and D) ZnO-R, (E and F) ZnO-F, and (G and H) ZnO-S. (A and B) Reproduced with permission from ref 45. Copyright 2007 Elsevier. (C−H) Reproduced with permission from ref 46. Copyright 2021 Elsevier.

the top and middle zones of the reactor, but as the intensity increased, it appeared around the horn tip.

The third step involved in the degradation process is related to the collapse of cavitation bubbles that produces high local temperature points. This leads to thermal activation of semiconductor surface, enhancing e^-/h^+ pairs production and formation of active radicals.[28,37] The produced $OH^\bullet$ radicals can diffuse in the bulk solution and reach the interfacial region of the other cavitation bubbles with high temperature due to the existence of a large gradient of temperature and radical concentration. Notably, through sonocatalytic decontamination processes, hydrophobic organic contaminants tend to move to interfacial regions and to be destroyed by the cavitation bubbles and highly concentrated $OH^\bullet$ radicals at the gas-bubble region. On the contrary, hydrophilic contaminants could not get oxidized in the bubble boundaries due to their tendency to move to the bulk area and get decontaminated indirectly through the hydroxyl-radical-producing reactions initiated by the cavitation process or by photocatalysts. The presence of dissolved oxygen can enhance the effect of the third step. Thermal dissociation of dissolved oxygen and water molecules in the cavitation bubbles convert them into active species (including $OH^\bullet$, $O_2^{\bullet -}$, $H^\bullet$ and $OOH^\bullet$ radicals) (eqs 10−18). Then, the as-produced reactive species can participate in decontamination processes in the bulk solution and/or at the gas−cavitation−bubble interface. In the case of absence of contaminants, the produced species convert to water molecules (eqs 15−17). The production of H_2O_2 occurs outside of hotspots (implosion of bubbles) or at the lower temperature gas−liquid interfaces by recombination of $OH^\bullet$ and $OOH^\bullet$ radicals in the same way as during the photocatalysis (eqs 6−9).[38−40]

$$H_2O \xrightarrow{US} OH^\bullet + H^\bullet \quad (10)$$

$$O_2 \xrightarrow{US} 2O^\bullet \quad (11)$$

$$OH^\bullet + O^\bullet \rightarrow OOH^\bullet \quad (12)$$

$$O^\bullet + H_2O \rightarrow 2OH^\bullet \quad (13)$$

$$H^\bullet + O_2 \rightarrow OOH^\bullet \quad (14)$$

$$OH^\bullet + H^\bullet \rightarrow H_2O \quad (15)$$

$$2OH^\bullet \rightarrow H_2O + O^\bullet \quad (16)$$

$$OOH^\bullet + OH^\bullet \rightarrow H_2O + O_2 \quad (17)$$

$$2H^\bullet \rightarrow H_2 \quad (18)$$

2.3. Catalyst Cleaning Effect and Recyclability Studies

There has been evidence that ultrasound shock waves can cause catalyst depoisoning and cleaning. This was reported by Disselkamp et al.[41] investigating the ultrasound impact on hydrogenation vs isomerization of 3-buten-1-ol in the presence of black palladium in water. This study showed that applying ultrasound during the reaction caused a rapid *in situ* cleaning reduction of black Pd. This was caused by the implosion of cavitation bubbles on the surface of Pd, which led to a 5-fold

https://doi.org/10.1021/acsnanoscienceau.2c00058
ACS Nanosci. Au 2023, 3, 103−129

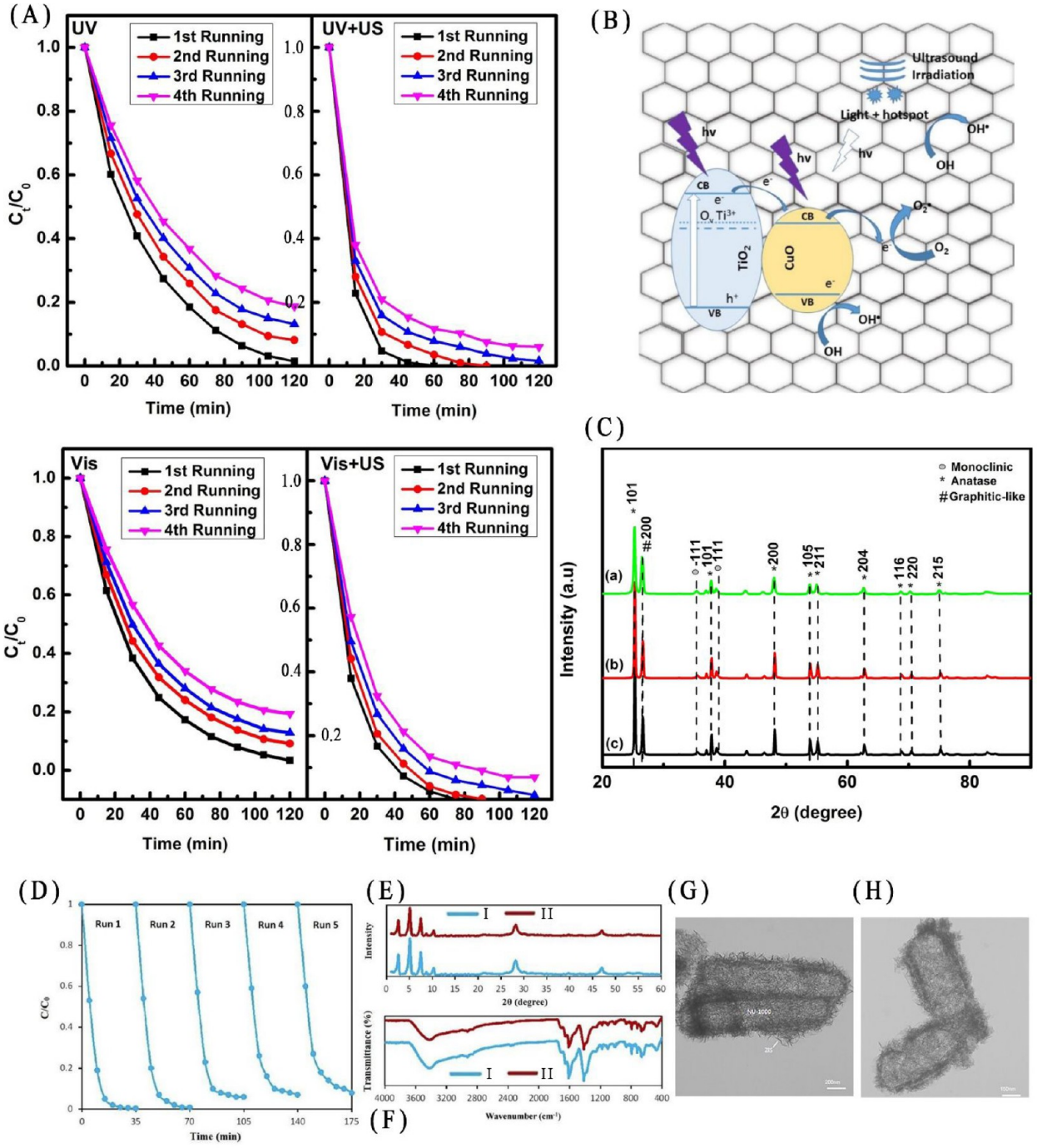

Figure 5. (A) Reusability test of TiO_2/CuO/NGP (1:0.1 10G) under different modes of light irradiation. (B) Schematic sonophotocatalytic charge transfer mechanism of integrated TiO_2/CuO/NGP. (C) XRD patterns of the sample (a) before treatment, (b) after photocatalytic treatment, and (c) after sonophotocatalytic treatment of MB. (D) Recyclability of NU@ZIS20 nanocomposite catalyst in sonophotocatalytic tetracycline degradation. (E) XRD patterns and (F) FT-IR spectra of NU@ZIS20 before (I) and after (II) sonophotocatalytic cyclic tests under a 300 W halogen lamp irradiation. TEM image of NU@ZIS20 nanocomposite before (G) and after (H) five runs. (A−C) Reproduced with permission from ref 51. Copyright 2018 Elsevier. (D−H) Reproduced with permission from ref 52 Copyright 2021 American Chemical Society.

increase in the reaction rate. The same phenomenon was observed by Carcenac et al.[42] studying catalytic hydrogenation of fluorinated alkenes using PtO_2.

In photocatalysis, physically, cavitation bubbles collapsing near the surface of nanoparticles will cause asymmetric shock waves, which consequently leads to deaggregation of particles and continuous surface cleaning, increasing the exposed active sites at the surface of the material.[43,44] Silva et al.[45] reported an improvement in the specific BET surface area of TiO_2 when H_2O_2-assisted sonophotocatalytic degradation of phenolic compounds in agro-industrial effluent was investigated. Although the pre- and post-treatment catalysts displayed similar type isotherms (Figures 4A,B), the used sample was able to adsorb much more nitrogen than the fresh one. After 180 min of reaction, the BET specific surface area improved from 47.3 to 109.7 m^2/g, and the average pore diameter increased from 20.1 to 27.7 nm, suggesting that the deaggregation of nanoparticles by ultrasound results in an

https://doi.org/10.1021/acsnanoscienceau.2c00058
ACS Nanosci. Au 2023, 3, 103−129

enhancement in surface area. The same phenomenon was observed by Yang et al.[46] when three different morphologies of ZnO nanoparticles were synthesized and employed for sonophotocatalytic degradation of methyl orange. Surface areas of rod-like ZnO (ZnO-R) with 2.617 m^2/g, flower-like ZnO (ZnO-F) with 14.98 m^2/g, and sheet-like ZnO (ZnO-F) with 47.46 m^2/g increased after the treatment. According to SEM images (see Figure 4C−H), there was no significant morphological change after the sonophotocatalytic process.

Reusability is one of the most prominent factors, influencing the application of nanomaterials as well as their economic aspects. During conventional photocatalytic reactions, sticking of pollutant molecules or degradation products onto the catalyst surface, in particular porous sites, leads to catalyst poisoning and, thereby, decreased efficiency over continuous use of the photocatalysts.[26] Reusability tests have revealed that photocatalysts can be reutilized generally over three to five consecutive cycles while maintaining approximately over 85% photocatalytic degradation efficiency. This usually depends on the type of nanomaterials used, pollutants and operational parameters. Usually, the catalyst samples were collected, washed with DI water, dried and gathered for next consecutive cycles.[47,48] For instance, Niu et al.[49] showed that boron-doped TiO_2, as a Vis-light-driven photocatalyst, could be used for five runs in the photocatalytic degradation of rhodamine B (RhB) under optimized conditions. The same number of cycles with about 80% degradation efficiency at the fifth one was obtained for the photocatalytic degradation of MB using WO_3/SiO_2 monoliths.[50]

Sonophotocatalysis, as an upgraded photocatalytic degradation method with a higher removal potential, enables catalysts to be more effectively reused. The generated acoustic waves, cavitation bubbles and subsequent shock waves can have refreshing and depoisoning effects, leading to better sonophotocatalysts recyclability without a significant decrease in efficiency.[43,44] Taufik et al.[51] examined the photocatalytic and sonophotocatalytic degradation of MB by a TiO_2/CuO composite incorporated with graphene nanoplates under both Vis and UV light irradiations. As can be seen in Figure 5A, catalysts showed better cyclic performances in both Vis + US and UV+US degradation experiments compared to those solely under Vis and UV illuminations. In the photocatalytic runs, catalysts were reused for four consecutive cycles with approximately 20% decrease in efficiency in both series of experiments. However, when using sonophotocatalysis, the degradation efficiency was maintained at 100% for the first three cycles. This is clear evidence of the beneficial effect of US waves in catalyst cleaning, which increased the number of active sites in the surface of the materials. On these active sites, high-energy photons will be continuously absorbed, giving electrons enough energy to migrate to the CB and initiate sonophotocatalytic oxidation reactions. The schematic sonophotocatalytic charge transfer pathway of $TiO_2/CuO/NGP$ is also shown in Figure 5B. The intensity and location of XRD peaks remained unchanged after six cycles (Figure 5C,a−c)), proving that ultrasonic cleaning has no destructive effect on the crystalline structure of the catalysts. In another study by Abazari et al.,[52] core@shell Zr (IV) metal−organic framework nanorods and $ZnIn_2S_4$ nanostars (NU@ZIS20) achieved a sonophotocatalytic activity of 92% for tetracycline degradation after five cycles (Figure 5D). There were not significant structural or morphological changes, as can be seen from the XRD patterns, Fourier transform infrared spectroscopy (FTIR) spectra, and TEM images in Figure 5E−H.

Hayati et al.[53] revealed that N, Fe codoped TiO_2@single-walled carbon nanotubes (CNTs) could be reused for seven cycles for ultra-assisted photocatalytic degradation of sulfathiazole. In a similar investigation by Gholami et al.,[54] Zn−Cu−Mg-mixed metal hydroxide/g-C_3N_4 (MMH/g-C_3N_4) was used for the degradation of sulfadiazine. A negligible decrease of 5% in performance was observed. Additionally, no fracture in the structure or mass loss was detected after 10 cycles.

3. NANOSTRUCTURED SONOPHOTOCATALYST ENHANCEMENT STRATEGIES

3.1. Catalyst Modifications

It is well-known that both the size and morphology of semiconductors play a crucial role in their properties.[55−57] Some examples of nanomorphologies are nanoparticles, nanorods, nanoflowers, nanotubes, and nanosheets. Due to the greater surface-to-volume ratio, availability of increased number of accessible active sites, and higher separation efficiency of photogenerated electrons and holes, nanoscaled catalysts tend to have higher performance when compared to non-nano or bulk materials.[58] However, limited light absorption, high e^-/h^+ recombination rate, and low adsorption rate are mostly inevitable in sonophotocatalysis. Thus, researchers have focused their attention in modifying nanoscale semiconductor materials to enhance their catalytic activity. To this end, we have identified three main strategies: (1) addition of metal/nonmetal dopants, (2) use of nanostructured organic/inorganic supports, and (3) the combination with other nanosized semiconductors.

3.1.1. Doping Strategy. Doping with metal/nonmetal ions was employed to improve the catalytic activity of nanomaterials through numerous sonophotocatalytic degradation investigations.[20,59,60] Metallic dopants increase catalytic performance by forming impurity energy levels in the band gap. Equations 19 and 20 describe how incorporated metallic ions participate in the photocatalytic process of semiconductors. Mt^n represents metallic ion-doped nanocatalysts. They help with photocatalysis process mainly on two aspects: (i) increasing photon-absorption from the light source and/or SL and (ii) considerably reducing the e^-/h^+ recombination rate. Additional electron and hole states are formed in the nanostructure, which facilitates the e^- and h^+ transfer between the metallic dopant and the nanosized semiconductor (see eqs 21 and 22).

$$Mt^{n+} \xrightarrow{SL/h\nu} Mt^{(n+1)} + e_{CB}^- \quad (19)$$

$$Mt^{n+} \xrightarrow{SL/h\nu} Mt^{(n-1)} + h_{VB}^+ \quad (20)$$

$$Mt^{n+} + h_{VB}^+ \rightarrow Mt^{(n+1)+}(\text{hole trap}) \quad (21)$$

$$Mt^{n+} + e_{CB}^- \rightarrow Mt^{(n-1)+}(\text{electron trap}) \quad (22)$$

Tabasideh et al.[20] synthesized Fe-doped TiO_2 pseudospherical nanoparticles for the degradation of diazinon as a persistent organophosphorus pesticide in aquatic media. They achieved considerably greater degradation efficiency (85%) than using pristine TiO_2 (reported to be ~50%) while using a sonophotocatalytic process. Similar results were obtained by Yap et al.[16] They degraded paracetamol by

https://doi.org/10.1021/acsnanoscienceau.2c00058
ACS Nanosci. Au 2023, 3, 103−129

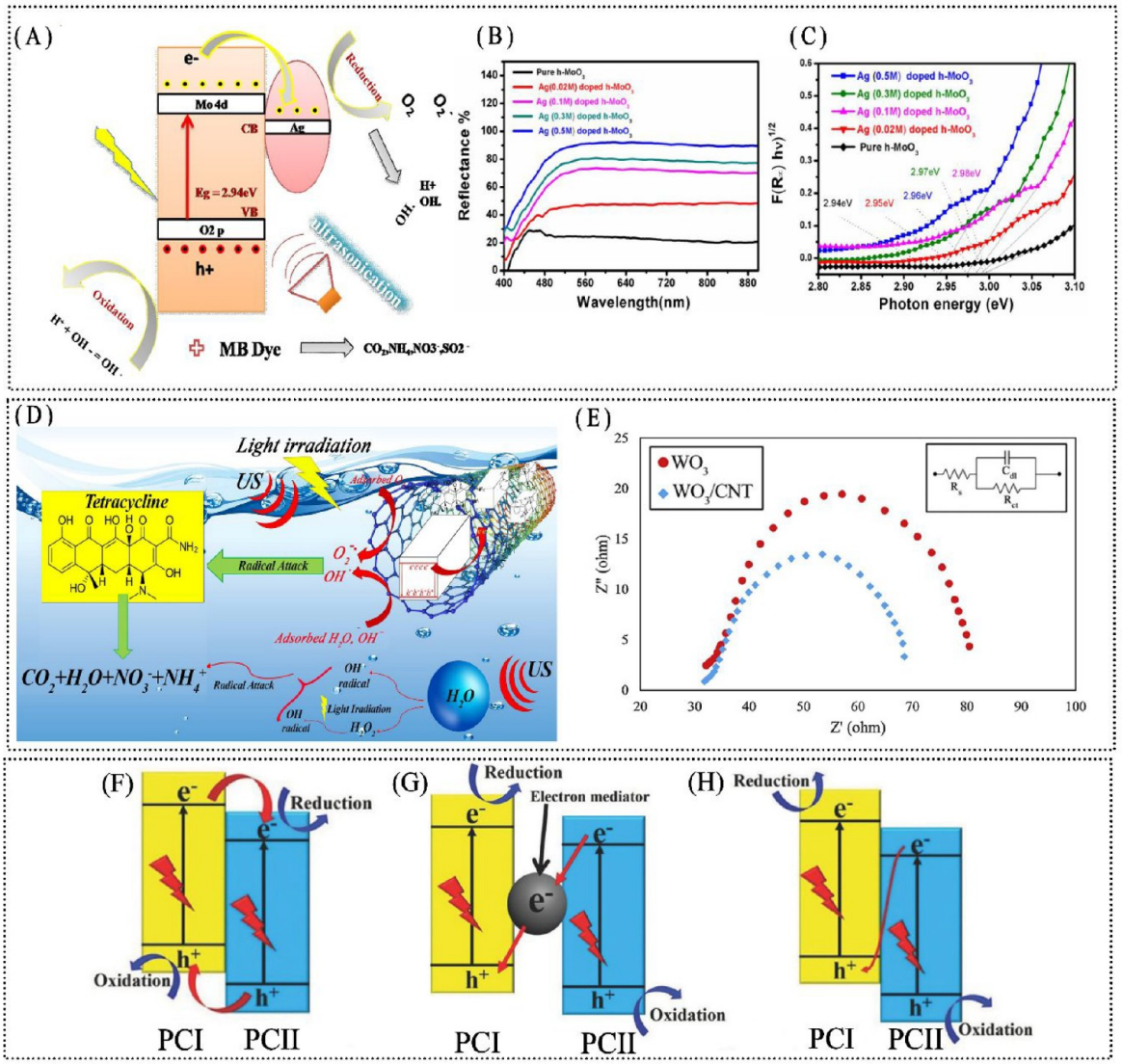

Figure 6. (A) Addition of dopants to achieve higher sonophotocatalytic potential: Ag-doped *h*-MoO_3 nanorods for the degradation of MB under diffused sunlight and ultrasonic irradiation. (B) Diffuse reflectance spectra (DRS) of MoO_3 and Ag-doped MoO_3 nanorods. (C) Tauc plots of MoO_3 and Ag-doped *h*-MoO_3 nanorods. (D) Introduction of nanosubstrates (CNTs) for catalytic performance improvement: WO_3/CNT nanocatalyst for the decontamination of tetracycline from aquatic solution. (E) EIS patterns of WO_3 and WO_3/CNT samples. (F) Type II heterojunction, (G) indirect Z-scheme using mediators, and (H) direct Z-scheme (mediator-free) charge transfer mechanisms at the interface. (A–C) Reproduced with permission from ref 61. Copyright 2017 Elsevier (D–E). Reproduced with permission from ref 71. Copyright 2020 Elsevier. (F–H) Reproduced with permission from ref 82. Copyright 2017 Wiley Online Library.

means of sonophotocatalysis using Fe-doped TiO_2 nanoparticles and achieved full 100% degradation efficiency in 30 min. They created trapping sites in the TiO_2 lattice, slowing down the e^+/h^- recombination rate. The doped catalyst exhibited ~2 times improvement compared to pristine TiO_2 in the sonophotocatalytic degradation process. Paul et al.[61] synthesized Ag-doped flower-like hierarchical molybdenum oxide (*h*-MoO_3) nanorods and utilized them for the degradation of MB under diffused sunlight and ultrasonic irradiation. As seen in Figure 6A, Ag acts as an electron trap, captures electrons that migrate to the CB of *h*-MnO_3 and suppress the e^-/h^+ recombination. The captured electrons can then react with oxygen to produce superoxide radicals. Ag-doped *h*-MnO_3 nanorods degraded 98% of MB in 90 min, while nondoped nanorods showed 97.8% degradation efficiency in 150 min. The 40% decrease in the reaction time clearly revealed the advantage of Ag doping. This can be explained with the reduction of the *h*-MoO_3 band gap and the dramatically increased absorption in the Vis region (see Figure 6B,C). Rajoriya et al.[62] employed Sm-doped TiO_2 for the acoustic cavitation-assisted photodegradation of 4-acetamidophenol. They reported ~30% enhancement in the 4-acetamidophenol degradation efficiency.

Non-metal dopants can also enlarge the absorption range of Vis light, significantly increase charge carriers' separation, and reduce e^-/h^+ recombination due to the introduction of localized electronic states above semiconductor's VB in the bandgap.[63] Kumawat et al.[64] synthesized an N-doped ZnO nanorod-like structure and employed it in the degradation of nigrosine under simultaneous ultrasonic and Vis light irradiations. The sonophotocatalytic degradation rate constants for N-doped and undoped ZnO were 7.33×10^{-4} and 4.6×10^{-4} s^{-1}, respectively. Rajoriya et al.[62] employed N-doped TiO_2 spherical nanoparticles with a porous structure for

https://doi.org/10.1021/acsnanoscienceau.2c00058
ACS Nanosci. Au 2023, 3, 103–129

acoustic cavitation assisted photodegradation of 4-acetamidophenol and also achieved a higher degradation efficiency (91%) compared to undoped TiO_2 (~79%). Additionally, sonophotocatalysis yielded a maximum degradation efficiency in 4-acetamidophenol under optimized conditions of 91% within 180 min. However, when using only photocatalytic oxidation, only 63% of degradation rate was achieved.

An additional strategy that a few groups have adopted is codoping.[17,53,65] This grants important synergic effects, changes both the transfer and recombination dynamics of charge carries, and shifts light adsorption spectra to the Vis light region due to interactions between dopants within the crystalline matrix of nanocatalysts.

3.1.2. Using Nanostructured Substrates. Loading nanoscale semiconductors onto nanostructured supports has been reported to be an effective strategy to improve the sonophotocatalytic performance of nanocatalysts. Nanostructured supports feature a high specific surface area. They can help prevent nanoparticle agglomeration, which is a quite common issue of nanoparticles, during the catalytic processes or washing/redispersion steps between cycles. Moreover, they provide a higher capacity for adsorption of organic pollutants and increase the chance of surface reactions as well as act as an acceptor of sono/photoinduced reactive species, significantly suppressing the e^-/h^+ recombination in nanoparticle catalysts.[66] Specifically, in sonophotocatalysis, continuous ultrasonic irradiation helps to reduce nanocatalyst agglomeration in solution to a certain extent. But, the negative side is that it may also cause the detachment of integrated nanocatalysts from the support. For example, Zeng et al.[19] reported a higher Mo leaching content of MoS_2 nanosheets grown on carbon layers in sonophotocatalytic elimination of levofloxacin when compared to the photocatalytic treatment employing peroxymonosulfate as an enhancer. Keeping this in mind, the nanocatalyst−substrate bonding should be sufficiently strong to avoid the nanocatalyst loss from the substrate surface to the solution and to increase the beneficial effect of the substrate's introduction. Hayati et al.[10] fabricated mesoporous hexagonal MgO nanocrystals onto CNT using a multistep fabrication method that started with the hydrothermal treatment of $Mg(NO_3)_2{\cdot}6H_2O$ and Na_2CO_3 followed with a calcination step and ultrasonic-assisted hydrothermal treatment. This nanocomposite was employed for the degradation of sulfadiazine (pharmaceutical pollutant) under ultrasonic and UV light irradiation, which exhibited 38.8% higher degradation efficiency than pristine MgO under the same conditions. The authors attributed the improved performance to the increased specific surface area, the reduction of e^-/h^+ recombination rate, and the inhibitory effect of CNTs as a substrate from agglomeration of MgO nanoparticles.

Zeolites are crystalline aluminosilicates with microporous (4−14 Å) structures that have been widely used as hybrid adsorbents and catalysts.[67,68] They possess unique chemical and structural properties including high surface area, high adsorption capabilities, and adjustable surface properties.[67] Having uniform pores and channel sizes, zeolites can serve as hosts for entrapping nanosized semiconductors and preventing the agglomeration of nanocatalysts.[69,70] Jorfi et al.[66] performed a comparative study on a sonophotocatalytic treatment of a textile industrial effluent using nanosized MgO spherical-shaped nanoparticles grafted on zeolite. The MgO@zeolite/UV/US system exhibited a much higher degradation rate (78%) than those of MgO/UV/US and MgO@zeolite/UV systems, with only 43%, and 49% elimination rates, respectively. These results highlight the importance of the zeolite as well as the binary use of US and UV systems to take advantage of both the sonocatalytic and photocatalytic mechanisms. Also, MgO nanoparticles showed a minimal loss of <0.3 mg/L after the treatment under optimum conditions, confirming the excellent physicochemical stability of MgO@zeolite in sonophotocatalysis processes.

Isari et al.[71] synthesized WO_3 nanocuboids coupled with CNTs for the decontamination of tetracycline, where CNTs acted as a substrate (see the molecular structure and charge transfer pathway in Figure 6D). They achieved the excellent introduction of CNTs into the WO_3 framework. The outstanding activity of this nanocomposite was demonstrated by the total elimination of tetracycline in 60 min, outperforming the individual photocatalytic and sonocatalytic processes with 48.56% and 45.92% degradation efficiencies. The reduced radius of the semicircle in electrochemical impedance spectroscopy (EIS) Nyquist plot revealed the increased interfacial charge transfer in the composite (Figure 6E). The authors believed that the interfacial bonding (W−C or/and W−O−C) formed between WO_3 and CNTs allowed for the photogenerated electrons to be transferred to CNTs with very low resistance. In this case, the substrate contributed to the catalytic performance by reducing the e^-/h^+ recombination rate.

3.1.3. Coupling with Other Semiconductors. Another promising strategy for increasing photon absorption from light source or SL is coupling a nanoscale semiconductor with another lower band gap semiconductor. When they are in contact with each other, semiconductors with different Fermi levels form heterojunctions at the interface, which leads to the formation of an internal electric field. This electric field can direct the movement of electrons and holes through the interfacial zone.[72,73] The most investigated and desired heterojunction for photocatalysis and sonophotocatalysis is known as type II. In the conventional type II heterojunction, the holes and electrons kinetically flow upward and downward, respectively, which effectively facilitates e^-/h^+ separation (Figure 6F). Aghaei et al.[74] synthesized ZnO/CuO spherical-shaped nanoparticles with an average particle size of 32 nm by coprecipitating zinc nitrate and copper(II) nitrate for the removal of parathion from wastewater. The total degradation of parathion was achieved after 60 min of simultaneous ultrasonic and light irradiation. They also evaluated the beneficial effect of the addition of CuO to ZnO crystalline nanostructure and found that a ZnO/CuO (90:10) mixture exhibited higher sonophotocatalytic activity than pure ZnO nanoparticles. Under optimized conditions, the sonophotocatalytic reaction rate constant was 1.36 times higher than that from photocatalysis. A similar charge transfer mechanism coupled with synergism between the UV and US processes was also shown by Eshaq et al.[75] in a study on hydrothermally prepared $FeVO_4$@BiOCl (nanorods/nanoflowers with a core@shell heterojunction structure) for the efficient sonophotocatalytic degradation of *p*-nitrophenol. Guo et al.[76] fabricated brush-like ZnO nanorod arrays on a stainless-steel mesh and subsequently transformed them into ZnO/ZnS core@shell nanorods and nanotubes to investigate the effectiveness of heterojunction and the sonophotocatalytic degradation capability for the MB removal. For over 50 min of reaction, the removal capability of ZnO/ZnS core@shell nanorods (45.4%) was remarkably higher than that of ZnO

https://doi.org/10.1021/acsnanoscienceau.2c00058
ACS Nanosci. Au 2023, 3, 103−129

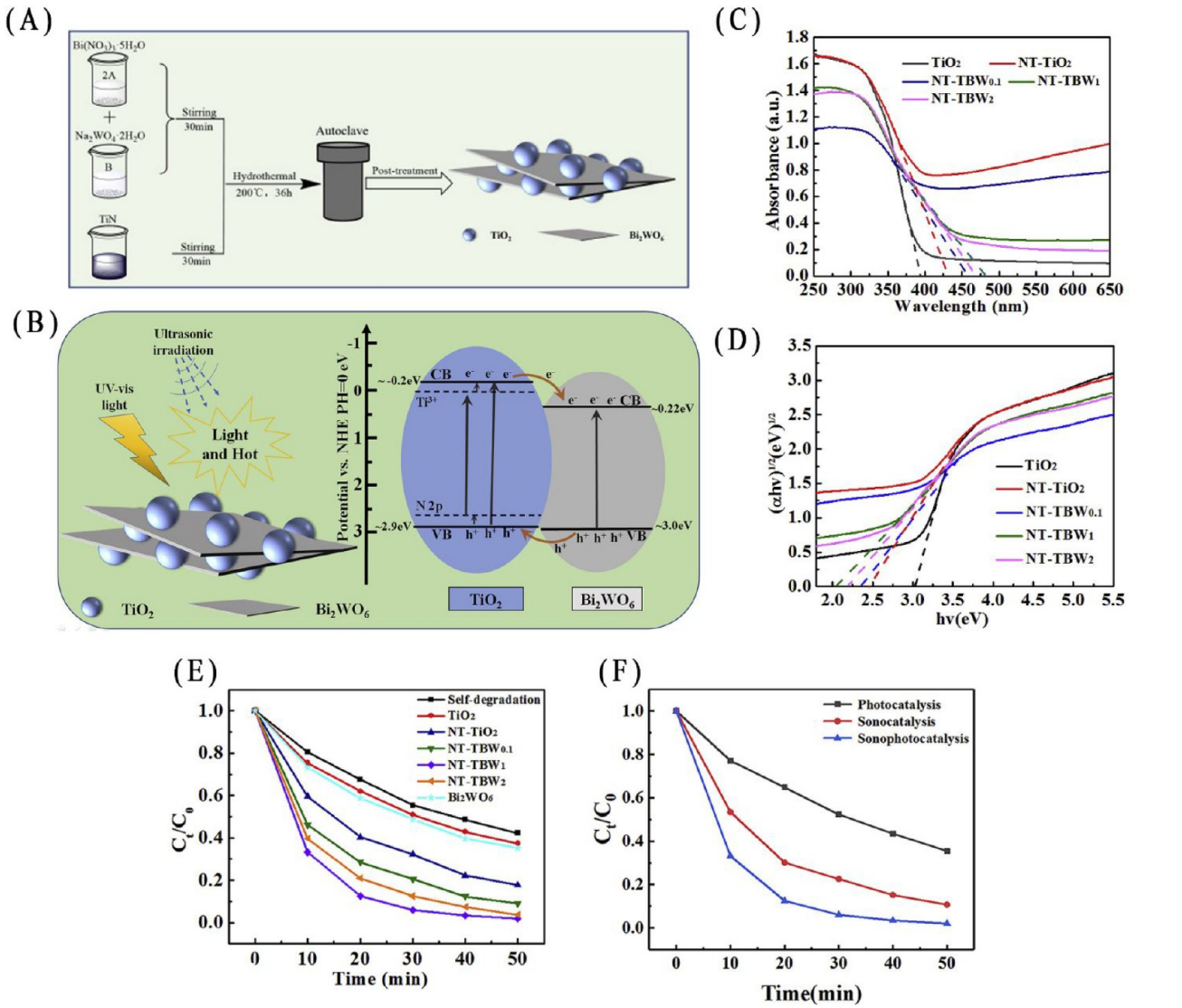

Figure 7. (A) Fabrication and (B) charge transfer mechanism of N/Ti^{3+} codoped biphasic TiO_2/Bi_2WO_6 composite heterojunctions for MB decontamination. (C) Diffuse reflectance spectrum and (D) Tauc plot of TiO_2, NT-TiO_2, and NT-TBW_x samples. (E) Sonophotocatalytic activities of Bi_2WO_6, TiO_2, NT-TiO_2, and different NT-TBW_x composite samples. (F) Comparative studies of sonophotocatalytic degradation of MB in different modes. Reproduced with permission from ref 17. Copyright 2020 Elsevier.

nanorods (25.1%), suggesting that the interfacial polarization field induced by the ZnO/ZnS heterojunction increased the sonophotocatalytic efficiency. As the nanorods were transformed into nanotubes, they exhibited a higher degradation rate (63.3%) due to the coupling effect of the enhanced piezoelectric field and the reduced migration distance, which suppressed the recombination of photoexcited electron−hole pairs. This study not only shed light on the importance of forming efficient heterojunctions in sonophotocatalysts but also indicated that morphology can play an important role in the performance of sonophotocatalysts.

Another interesting, increasingly explored charge transfer mechanism is indirect Z-scheme type, through which the excited electrons of photocatalyst II (PCII) are transferred downward to recombine with the holes on photocatalyst I (PCI) using an electron mediator (Figure 6G). These mediators can be either conductors (i.e., metal nanoparticles, CNT or graphene), which act as low resistive electron highways or redox pairs (i.e., Co^{3+}/Co^{2+} and Fe^{3+}/Fe^{2+}).[77,78] In Z-scheme systems, unlike conventional type II heterojunction composites, the reduction and oxidation reactions are driven by electrons at the CB of PCI with a higher redox potential and holes located at the VB of PCII with a higher oxidation potential, respectively.[79]

The recently emerged direct Z-scheme catalytic systems, without engaging any mediators, have also been applied to both sonocatalysis and photocatalysis and demonstrated outstanding catalytic properties. The charge transfer mechanism is exactly the same as the above-mentioned indirect Z-scheme heterojunction (Figure 6H).[80,81] The electrons left at the CB of PCI and holes at the VB of PCII, with the highest reduction and oxidation potentials, respectively, are capable of participating in radical-producing reactions much more effectively. However, in the direct Z-scheme heterojunction, the shielding effect and the backward reactions are mostly hindered due to the absence of mediators.[82] In spite of all these favorable factors, rational construction of the direct Z-scheme system with an intimate interface and effective charge transfer remains challenging. It should be also mentioned that there are many articles on the Z-scheme sonocatalytic or photocatalytic

https://doi.org/10.1021/acsnanoscienceau.2c00058
ACS Nanosci. Au 2023, 3, 103−129

processes, but to the best of our knowledge there is no available comprehensive information about the integrated Z-scheme sonophotocatalytic systems, which may be worthwhile to be investigated in detail in future studies.

It is common to use the combination of these modification strategies for the fabrication of desirable sonophotocatalysts. Sun et al.[17] fabricated N/Ti^{3+} codoped biphasic TiO_2/Bi_2WO_6 composite heterojunctions (denoted as NT-TBW$_x$) by a single hydrothermal treatment (see Figure 7A), for the decontamination of MB, *p*-nitrophenol, RhB, and levofloxacin. The nanocomposite was composed of nanoparticles of biphasic TiO_2 (both anatase and rutile phases) and Bi_2WO_6 nanosheets with a lamellar structure. Although TiO_2 is a UV light responsive photocatalyst, N atoms and Ti^{3+} can create impurity levels above the VB and continuous local states below the CB of TiO_2, respectively (see Figure 7B). Both can result in TiO_2 exhibiting the Vis light response. Results shown in Figure 7C,D confirm that the band gap value of TiO_2 was reduced from 3.10 to 2.47 eV by incorporating N/Ti^{3+} and that the resulting catalysts absorbed both UV and Vis light. The combined effect of dopants and the charge transfer mechanism at the interface TiO_2/Bi_2WO_6 resulted in superior performance compared to other samples. Figure 7E depicts the comparative study that confirmed the synergistic effect among the heterojunctions, heterophase junction (anatase/rutile), and doping level. Since codoped composite samples (NT-TBW$_x$) had a higher light response and e^-/h^+ separation rate, their sonophotocatalytic performance was superior to that of N/Ti^{3+} codoped TiO_2 and pure TiO_2. In addition, the improved sonophotocatalytic degradation performance showed a positive synergism between sonocatalysis and photocatalysis (see Figure 7F). Over 50 min of reaction time, the degradation rate of MB by the sonophotocatalytic process is 98%, which is 1.09- and 1.52-fold greater than the degradation rates by sonocatalytic and photocatalytic techniques alone.

Babu et al.[83] fabricated CuO-TiO_2/rGO (rGO: reduced graphene oxide) for ultrasonic-assisted photocatalytic degradation of methyl orange dye. They found that both graphene oxide nanosheets and Cu played a crucial role in the system due to (i) band gap energy shifting from 3.23 to 3.08 eV as a function of Cu loading; (ii) rGO acting as electron acceptor and transfer bridge, improving charge mobility; and (iii) rGO providing a highly active surface area for the effective adsorption of organic pollutants. Similarly, such improvements made by the combination of these strategies have been reported in the literature.[27,53]

3.2. Process Modifications

Any additional source for generating reactive species can boost sonophotocatalytic activities. In the following, various process enhancement techniques are described.

The sparging of gases (N_2, Ar, O_2) enhances the performance of the system by generating high-potential bubble formation sites. This increases the rate of cavitation events and greatly influences the amount of produced H_2O_2, which can indeed actively participate in and contribute to the photocatalytic degradation process. Therefore, the number of cavitation bubbles will be in a direct relationship with the amount of sparged gas. Previous studies confirmed the positive effect of aeration on ultrasonic-produced degradation mechanisms.[15,84] It has been shown that Ar offers a better performance compared to N_2 thanks to its better solubility in water and a higher heat capacity ratio.[85] Another possible reason for relatively lower performance is N_2's scavenging effect, leading to less reactive species available for the photocatalytic reaction. Moreover, as shown in previous sections, O_2 can act as a scavenger agent for excited electrons on the CB, results in more production of $O_2^{\bullet -}$ and diminish the rate of e^-/h^+ recombination. Also, by further reacting with other existing species in solution, extra amounts of radicals like $HO_2^\bullet$ will be generated (eqs 23−25).

$$O_2 + e^- \rightarrow O_2^{\bullet -} \tag{23}$$

$$H_2O \xrightarrow{US} H^\bullet + OH^\bullet \tag{24}$$

$$O_2 + H^\bullet \rightarrow HO_2^\bullet \tag{25}$$

The ultrasonic-produced shock waves have a positive effect on boosting the production of reactive agents in the solution and enhancing the influence of aeration as an intensifier (eqs 26−28).[86]

$$O_2 \xrightarrow{US} 2O^\bullet \tag{26}$$

$$O^\bullet + HO_2^\bullet \rightarrow OH^\bullet + O_2 \tag{27}$$

$$O_2 + O^\bullet \rightarrow O_3 \tag{28}$$

To investigate the effect of gas purging, Dinesh et al.[85] selected a solution of 10 ppm of Basic Brown 1 dye for sonophotocatalytic treatment system using Fe-doped Bi_2O_3. Each experiment was carried out by bubbling the reaction mixture with Ar, air, O_2, and N_2, separately. According to the results, Ar bubbling exhibited the highest decontamination performance of 17% for 37 kHz, 13% for 22 kHz, and 8% for the UV-only case. These efficiencies were higher than those of N_2, air, and O_2. The overall positive synergism was also observed in the integrated sonophotocatalytic system.

By using H_2O_2 as an individual enhancer, a large number of free and adsorbed radicals can be released in the medium. Besides, it can act as an electron trap to suppress e^-/h^+ recombination (eqs 29−32).[87]

$$H_2O_2 \xrightarrow{h\nu/SL/US} 2OH^\bullet_{free} \tag{29}$$

$$H_2O_2 + e^- \rightarrow OH^- + OH^\bullet_{ads} \tag{30}$$

$$H_2O_2 + OH^\bullet \rightarrow H_2O + HO_2^\bullet \tag{31}$$

$$H_2O_2 + O_2^{\bullet -} \rightarrow OH^- + OH^\bullet + O_2 \tag{32}$$

Rahman et al.[60] explored the effect of H_2O_2 addition on the chemical oxygen demand (COD) removal of palm oil mill effluent using C−N codoped black TiO_2 under Vis light and US irradiations. According to the obtained results, the sonophotocatalytic elimination of COD improved from 67.69% to 75.48% by the addition of 1.0 mM H_2O_2. When the H_2O_2 concentration was increased to 2.0 mM, the COD removal efficiency rate went up to 84.63%. However, as H_2O_2 increased beyond 2.0 mM, the removal efficiency decreased dramatically, which was attributed to the radical scavenging effect of H_2O_2 molecules.

Owing to the high oxidation potential of O_3 (~2.08 eV), ozonation has been utilized for production of reactive species either alone or as an enhancer in combination with US-activated or/and light-activated degradation systems.[88,89] A series of reactions will be initiated be the presence of O_3 (eqs 33−37).

https://doi.org/10.1021/acsnanoscienceau.2c00058
ACS Nanosci. Au 2023, 3, 103−129

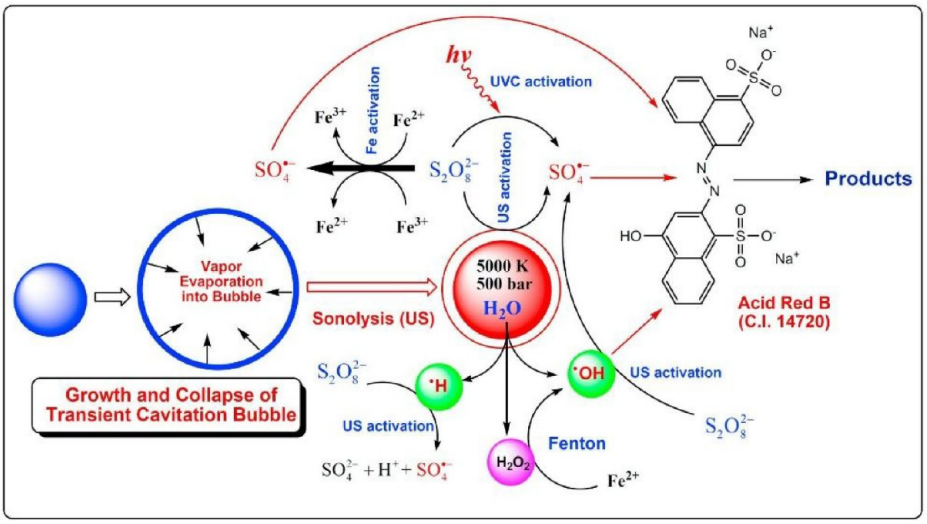

Figure 8. Schematic illustration of enhancer-enhanced sonophotocatalytic degradation of Azorubine dye using PDS and Fe^{2+}. Reproduced with permission from ref 93. Copyright 2017 Elsevier.

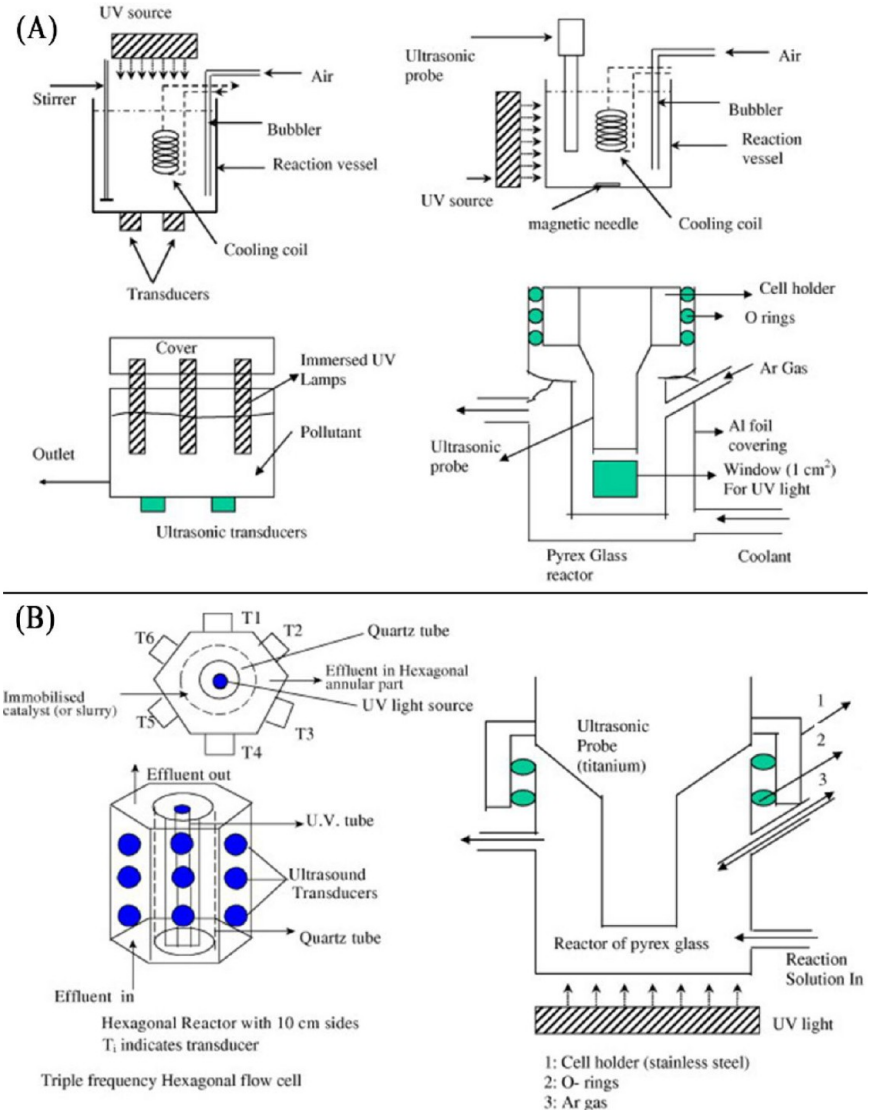

Figure 9. Some of the typical (A) batch and (B) continues sonophotocatalytic reactors. Reproduced with permission from ref 89. Copyright 2004 John Wiley and Sons.

https://doi.org/10.1021/acsnanoscienceau.2c00058
ACS Nanosci. Au 2023, 3, 103−129

$$O_3 + h\nu/\text{ultrasonic} \rightarrow O_2 + O \quad (33)$$

$$O + H_2O \rightarrow 2OH^{\bullet} \quad (34)$$

$$O_3 + OH^{\bullet} \rightarrow HO_2^{\bullet} + O_2 \quad (35)$$

$$HO_2^{\bullet} \rightarrow O_2^{\bullet -} + H^+ \quad (36)$$

$$OH^{\bullet} + O_2^{\bullet -} \rightarrow OH^- + O_2 \quad (37)$$

Acoustic streaming and turbulence generated by US waves can effectively break the mass transfer boundaries associated with ozonation, leading to further adsorption of O_3 in the solution. It is also notable that the existence of H_2O_2 species enlarges the share of O_3 in production of reactive agents in the solution (eqs 38 and 39).

$$H_2O_2 \rightarrow HO^{2-} + H^+ \quad (38)$$

$$O_3 + HO^{2-} \rightarrow O_2^{\bullet -} + OH^{\bullet} + O_2 \quad (39)$$

Sulfate radicals with excellent oxidizing potential (2.6−3.1 V) can be released in the solution by activation of peroxydisulfate (PDS) and peroxymonosulfate (PMS) enhancers.[90,91] Both of them release sulfate radicals (with higher oxidation potentials than $OH^{\bullet}$ (1.8−2.7 V)) and react with other ions in the solutions to produce $OH^{\bullet}$.[54] Ultrasonication waves can also degrade persulfate species into sulfate radicals according to eqs 40−47.

$$S_2O_8^{2-} \xrightarrow{\text{US}} 2SO_4^{\bullet -} \quad (40)$$

$$S_2O_8^{2-} + O_2^{\bullet -} \rightarrow SO_4^{2-} + SO_4^{\bullet -} + O_2 \quad (41)$$

$$HSO_5^- \xrightarrow{h\nu/\text{SL}} SO_4^{\bullet -} + O_2 \quad (42)$$

$$HSO_5^- + e^- \rightarrow OH^{\bullet} + SO_4^{2-} \quad (43)$$

$$HSO_5^- + e^- \rightarrow OH^- + SO_4^{\bullet -} \quad (44)$$

$$HSO_5^- + h^+ \rightarrow SO_5^{\bullet -} + H^+ \quad (45)$$

$$2SO_5^{\bullet -} + h^+ \rightarrow 2SO_4^{\bullet -} + O_2 \quad (46)$$

$$SO_4^{\bullet -} + OH^- \rightarrow OH^{\bullet} + SO_4^{2-} \quad (47)$$

Fenton-like reactions could provide the reaction media with extra numbers of radical species. Ferrous ions react with *in situ*-produced H_2O_2 during sonophotocatalytic reactions to provide additional free radicals and facilitate the degradation of dissolved organics. An optimum amount of Fe^{2+} could be converted to Fe^{3+} by reacting with H_2O_2 in the presence of UV or/and US to produce $OH^{\bullet}$ (eqs 48−52).[38]

$$Fe^{3+} + H_2O_2 \rightarrow Fe(OOH)^{2+} + H^+ \quad (48)$$

$$Fe(OOH)^{2+} \xrightarrow{h\nu/\text{SL}} Fe^{2+} + OH^{\bullet} \quad (49)$$

$$Fe(OOH)^{2+} \rightarrow Fe^{2+} + HO_2^{\bullet} \quad (50)$$

$$Fe^{2+} + O_2 \rightarrow Fe^{3+} + O_2^{\bullet -} \quad (51)$$

$$Fe^{2+} + H_2O_2 \rightarrow Fe^{3+} + OH^{\bullet} + OH^- \quad (52)$$

However, the excessive amount of Fe^{2+} could diminish catalytic activity due to its competition with organic materials, which tend to react with radical species in the solution.[92] It can also quench radicals when used simultaneously with PDS or PMS. For example, Chakma et al.[93] reported a clear schematic synergy function of Fe^{2+} and PDS enhancers when used in the degradation of Azorubine dye (Figure 8). They also confirmed that $SO_4^{\bullet -}$ can be scavenged by Fe^{2+} ions.

3.3. Reactor Design

Reactor design is considered one of the main factors in developing sonophotocatalytic treatment systems, influencing both process efficiency and overall cost of a system. Parts A and B of Figure 9 show some of the batch and continuous sonophotocatalytic reactors reported so far.[28,89] Some key features should be taken into account in their design to reach maximum efficiency.[15,89,94] The first one is the light source mode. It is notable that the type of light irradiation (indirect or direct) does not influence the synergism, giving considerable flexibility in their design. However, two other points must be taken into consideration: (i) uniform irradiation must be delivered to all the particles inside the reaction solution and (ii) light and US must be applied simultaneously rather than sequentially. Second, in terms of reactor type, continuous- or/and recirculation-equipped reactors are preferred in wastewater treatment compared to batch reactors due to higher treatment capacity, feasibility, and scale-up potential. Nevertheless, in terms of instrument cost, continuous reactors are more expensive than batch reactors in general, because they involve more system components. When lower doses of photocatalysts are used or/and photocatalyst separation is easy, slurry reactors can be used; otherwise, supported or immobilized catalyst reactors are preferred.[94] Multiple-frequency sonophotocatalytic reactors achieve higher efficient decontamination of wastewaters compared to single transducer or/and frequency operation, given their more uniform and intense energy transfer. Ye et al.[95] found that cavitation bubbles are much easier to collapse in dual-frequency ultrasonic field than those operated in the single-frequency mode.

4. SYNERGY

Employing the above-mentioned photo- and sono-activated mechanisms by combining photocatalysis and sonocatalysis lead to excellent synergistic effects on pollutant removal, which would not be achieved by applying them individually. As a quantitative measurement to evaluate the enhancement factor of integrated systems, the synergism between the processes can be calculated by the following equations:[38]

$$\text{synergy index} = \frac{K_{(X+UV+US)}}{K_{(X+UV)} + K_{(X+US)}} \quad (53)$$

$$\text{synergy (\%)} = \frac{K_{(X+UV+US)} - (K_{(X+UV)} + K_{(X+US)})}{K_{(X+UV+US)}} \times 100 \quad (54)$$

where $K_{(X+UV)}$, $K_{(X+US)}$, and $K_{(X+UV+US)}$ denote the reaction rate constants of photocatalytic, sonocatalytic, and sonophotocatalytic reactions and X is the type of catalyst. It should be noted that, to avoid any possible false conclusions, all formulas should be calculated by reaction rate constants instead of degradation percentages. Accordingly, by addition of additives and enhancers, the above-mentioned formula would be converted to eq 55.[19]

https://doi.org/10.1021/acsnanoscienceau.2c00058
ACS Nanosci. Au 2023, 3, 103−129

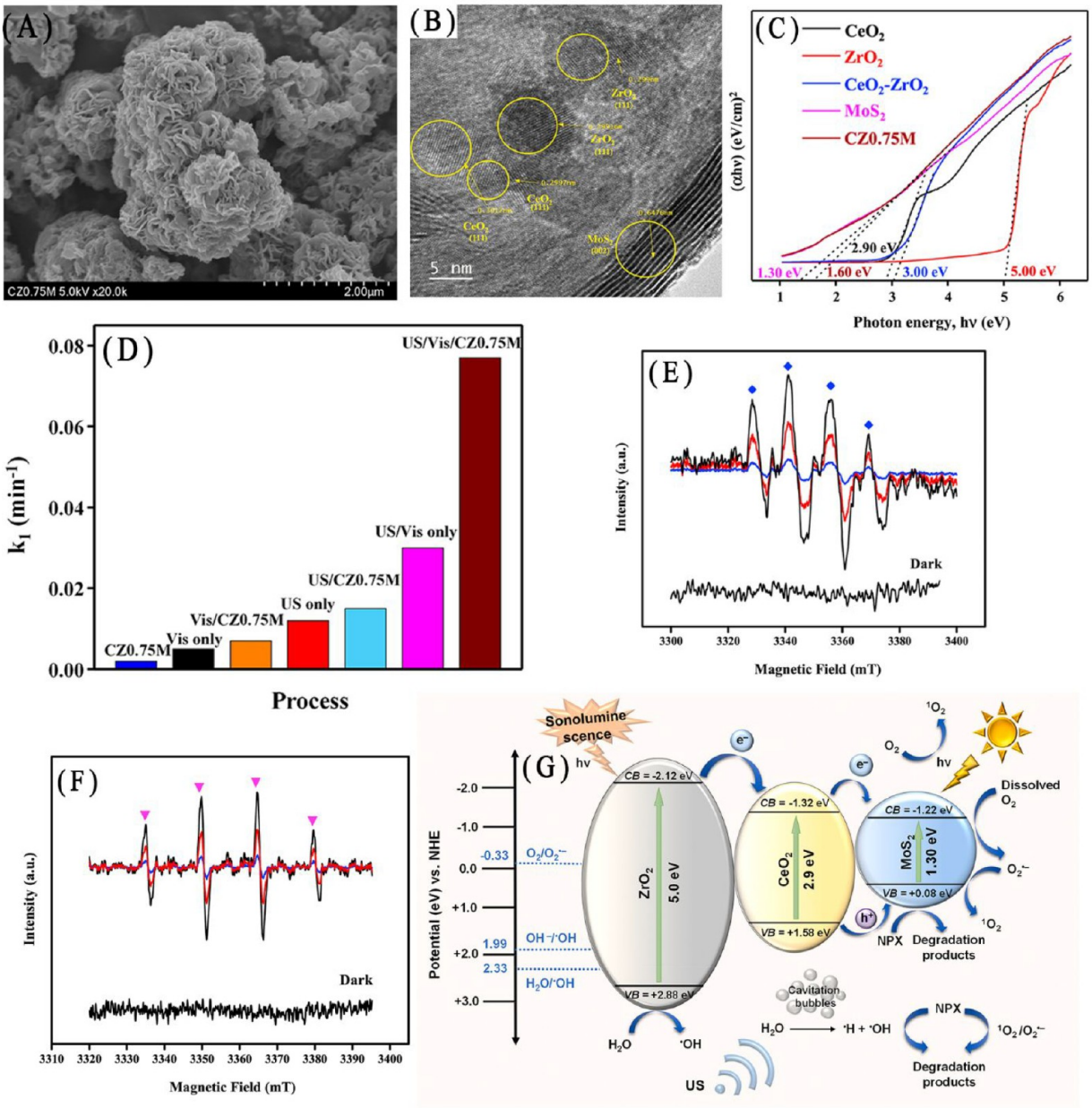

Figure 10. (A) SEM and (B) TEM images of CZ0.75 M. (C) Tauc plots of ZrO_2, CeO_2, MoS_2, CeO_2–ZrO_2, and CZ0.75 M. (D) Pseudo-first-order reaction rate constants of naproxen sonophotocatalytic degradation reactions in controlled experiments under optimum experimental conditions (catalyst dosage, 0.5 g/L, pH = 5.8; initial naproxen concentration, 10 mg/L; US frequency, 970 kHz; US power, 300 W; and light intensity, 0.17 mW/cm^2. ESR spectra of (E) DMPO-OOH and (F) DMPO-OH spin adducts under Vis (blue), US (red), and US/Vis (black) irradiations. (G) Schematic charge transfer mechanism of CZ0.75 M and sonophotocatalytic degradation of naproxen. Reproduced with permission from ref 98. Copyright 2021 Elsevier.

$$\text{synergy index} = \frac{K_{(X+Y+UV+US)}}{K_{(X+Y+UV)} + K_{(X+Y+US)}} \quad (55)$$

Eshaq et al.[96] reported a great synergism between binary irradiation of UV and US leading to complete decontamination of 4-nitrophenol (20 mg/L) using $FeVO_4$@CeO_2 (0.1 g/L) as the catalyst and H_2O_2 (10 mM) as an enhancer at pH = 7. Clearly, combining sonolysis with photocatalytic technique coupled with H_2O_2 and heterogeneous Fenton reaction shortened the reaction time to 30 min with excellent synergy percentage of 28.9% (using eq 54). A study by Lops et al.[58] shows that coupling sunlight and ultrasonic irradiation in a sonophotocatalytic approach resulted in complete removal of RhB in just 10 min by using micro- and nanosized ZnO as catalysts, demonstrating an excellent synergy between the two individual processes. This impact was shown by the great increase in the kinetic rate constant of about 56 and 13 times. In addition, there was a notable decrease of the half-lifetime (the required time to eliminate the 50% of the initial RhB concentration) of about 98% and 92%, compared to sole sonocatalytic and photocatalytic systems, respectively. Selvamani et al.[97] reported a synergy value of 3.83 and 1.71 for sonophotocatalytic degradation of tetracycline and ciprofloxacin antibiotics when using a Cu_2O/MoS_2/rGO nanocomposite within short times of 10 and 75 min, respectively.

https://doi.org/10.1021/acsnanoscienceau.2c00058
ACS Nanosci. Au 2023, 3, 103−129

Table 1. Summary of Cost Estimation of Photocatalytic, Sonocatalytic, and Sonophotocatalytic Degradation of Contaminants[14,19,75,97,98,105−109] [a]

					Reaction rate constant (min^{-1})			Energy power (W)			E_{EO} (kWh/m³ * order)			Costs ($)				
Power source	Enhancer	Catalyst	Contaminant	V solution (L)	K UV/cat	K US/Cat	K (UV/US/Cat)	P_{UV}	P_{US}	P (UV/US/Cat)	E_{EO} UV/Cat	E_{EO} US/cat	E_{EO} (UV/US/Cat)	Cost UV/Cat	Cost US/Cat	Cost (UV/US/Cat)	Synergy index	Ref
Halogen lamp + 40 kHz US bath	--	Cu_2O/MoS_2/rGO	Tetracycline	0.1	0.03	0.018	0.184	150	120	270	1920	2560	563.479	184.3	245.8	54.1	3.83	[97]
160 Hg 420 nm lamp + 20 kHz titanium probe sonicator	--	ZnO/CNT	MB	0.1 for UV/ 0.2 for US	0.015	0.0171	0.0198	160	60	220	4096	673.684	2133.333	393.2	64.7	204.8	0.617	[105]
160 W Hg lamp 420 nm filter	H_2O_2 assisted	ZnO/CNT	4- nitrophenol	0.1 for UV/ 0.2 for US	0.06	0.15	0.3	160	60	220	1024	76.8	140.8	98.3	7.4	13.5	1.429	[106]
High-pressure Xe lamp+ bottom US generator (40 kHz)	PMS assisted	MoS_2	Levofloxacin	0.1	0.0239	0.0022	0.0389	2.4	70	72.4	38.561	12218.182	714.694	3.7	1172.9	68.6	1.49	[19]
		MoS_2/C	Levofloxacin	0.1	0.0247	0.0021	0.0702	2.4	70	72.4	37.312	12800	396.034	3.6	1228.8	38	2.62	
16w UVC lamp + bottom US transducer	--	P25	Bisphenol A	1.1	0.006	0.007	0.028	16	50	66	93.090	249.351	82.286	8.9	23.9	7.9	2.154	[107]
8W UVC lamp +13 mm titanium probe	Fenton assisted	$FeVO_4$@BiOCl	p-nitrophenol	0.11	0.0403	0.031	0.112	8	125	133	69.298	1407.625	414.545	6.7	135.1	39.8	1.571	[75]
6W UVC lamp +125 W US wave 13 mm titanium prob	Fenton assisted	FeOCl (I)	Nitrobenzene	0.11	0.0479	0.0217	0.0892	6	125	131	43.727	2010.8923	512.678	4.2	193	49.2	1.28	[108]
		CuOCl (II)			0.0373	0.0161	0.0635				56.154	2710.333	720.172	5.4	260.2	69.1	1.189	
		BiOCl (IV)			0.03	0.0141	0.0484				69.818	3094.778	944.853	6.7	297.1	90.7	1.091	
		ZnOCl (III)			0.0259	0.0115	0.0426				80.870	3794.466	1073.495	7.8	364.3	103.1	1.139	
25 W UVC lamp +4 cm in diameter pizo-electeriz disk as US irradiation source	--	$FePO_4$	Methyl violet 2B	0.5	0.0229	0.0068	0.0397	25	80	105	83.843	903.529	203.123	8.1	86.7	19.5	1.33	[109]
14.4 W/m blue LED light+95 W US bath	--	Ce:Cu-1,4-BDO AH2	Diazinon	0.05	0.138	0.059	0.279	14.4	95	109.4	80.139	1236.610	301.144	7.7	118.8	28.9	1.41	[14]
240 W LED lamp US bath (Ultech, 40 and 970 kHz, 300 W)	-	CeO_2–ZrO2@MOS_2	Naproxen	0.05	0.007	0.014	0.077	250	300	550	27428.571	16457.143	5485.714	2633.1	1579.9	526.6	3.67	[98]

[a]Electricity rate was assumed to be $0.096 per kWh according to average electricity price for businesses in Canada, March 22. Source: www.globalpetrolprices.com. Materials' costs are not included.

Talukdar et al.[98] constructed CeO_2−ZrO_2@MoS_2 (CZ0.75 M) nanoflowers for naproxen sonophotocatalytic degradation. The morphological characteristics of the hybrid nanostructure CZ0.75 M were validated by field emission scanning electron microscopy (FESEM) micrographs and TEM images (Figure 10A,B). CeO_2−ZrO_2 hybrids were grown uniformly between and on the exterior of the MoS_2 nanosheets in the CZ0.75 M. The CZ0.75 M ternary composite has a band gap of 1.60 eV lower, when compared to ZrO_2, CeO_2, and CeO_2−ZrO_2 (Figure 10C). The low band gap energy of MoS_2 (1.30 eV) shortened the overall band gap of the hybrid material by interaction with CeO_2−ZrO_2 and defect energy states. The presence of these defects and oxygen vacancies from Ce^{3+} formation not only promoted a rapid charge carrier migration but also maximized the solar spectrum utilization. The sonophotocatalytic degradation of naproxen by the CZ0.75 M achieved 96% degradation efficiency within 40 min. It had a synergistic effect of 72.7%, resulting in 11- and 5.5-times greater degradation efficiencies than the individual sonocatalytic and photocatalytic experiments, respectively (Figure 10D). According to the electron spin resonance (ESR) results shown in Figure 10E,F, in the US/Vis/CZ0.75 M system, DMPO-OOH (DMPO: 5,5-dimethylpyrroline-*N*-oxide) and DMPO-OH spin adduct signals were stronger than in the Vis and US alone system. US irradiation of the solution resulted in SL and the conversion of microbubble cavitation energy into optical energy, which enhanced the production of radical species. Figure 10G shows the schematic charge transfer mechanism of the CZ0.75 M and sonophotocatalytic degradation of naproxen. As seen, by forming an efficient ternary heterojunction among CeO_2, ZrO_2, and MoS_2, electrons can easily migrate through the interfaces, reducing charge recombination. Electrons on the CB of MOS_2 can easily react with O_2 to produce radical species and holes at the VB of ZrO_2 can form $OH^{\bullet}$ species by reacting with water molecules.

5. ELECTRICAL ENERGY CONSUMPTION

In full-scale applications, the available resources and economic considerations are of high importance. Only a limited number of articles have been published on the sonophotocatalysis for wastewater treatment.[13,64] Little is known about the economic aspects of this technique. In advanced oxidation processes (AOPs), the amount of electrical energy consumed is responsible for the major fraction of operating expenses. Using an extra electrical-energy-consuming source—ultrasonic device—in addition to the traditional photocatalytic system may raise questions about the performance and cost-effectiveness. Defined by Bolton et al.[99] and approved by IUPAC, the figures-of-merit of AOPs can be calculated for electrical-energy-driven systems numerically. These calculations are divided into two types: (i) electrical energy per mass (E_{EM}) and (ii) electrical energy per order of magnitude (E_{EO}), which are suitable for situations where pollutant concentration is high and low, respectively. E_{EO} is the electric energy in kilowatt hours [kWh] required to remove a pollutant by 1 order of magnitude (90%) in a unit volume [e.g., 1 m^3] of polluted air or water. Low concentrations of contaminants and first-order degradation reactions are the prerequisites for using E_{EO} to determine the electrical energy consumption of an AOP system. The pseudo-first order kinetics of a sonophotocatalytic reaction system can be described according to eq 56. Also, the E_{EO} (kWh/m^3·order) for an AOP can be calculated by eq 57.[60]

$$\log\left(\frac{[C_0]}{[C]}\right) = 0.4343K_{app}t \tag{56}$$

$$E_{EO} = \frac{1000 \times P_e \times t}{60 \times V \times \log\left(\frac{[C_0]}{[C]}\right)} \tag{57}$$

where K_{app} (min^{-1}) is the pseudo-first order rate constant, P_e denotes the input power of electrical-energy-consuming source

https://doi.org/10.1021/acsnanoscienceau.2c00058
ACS Nanosci. Au 2023, 3, 103−129

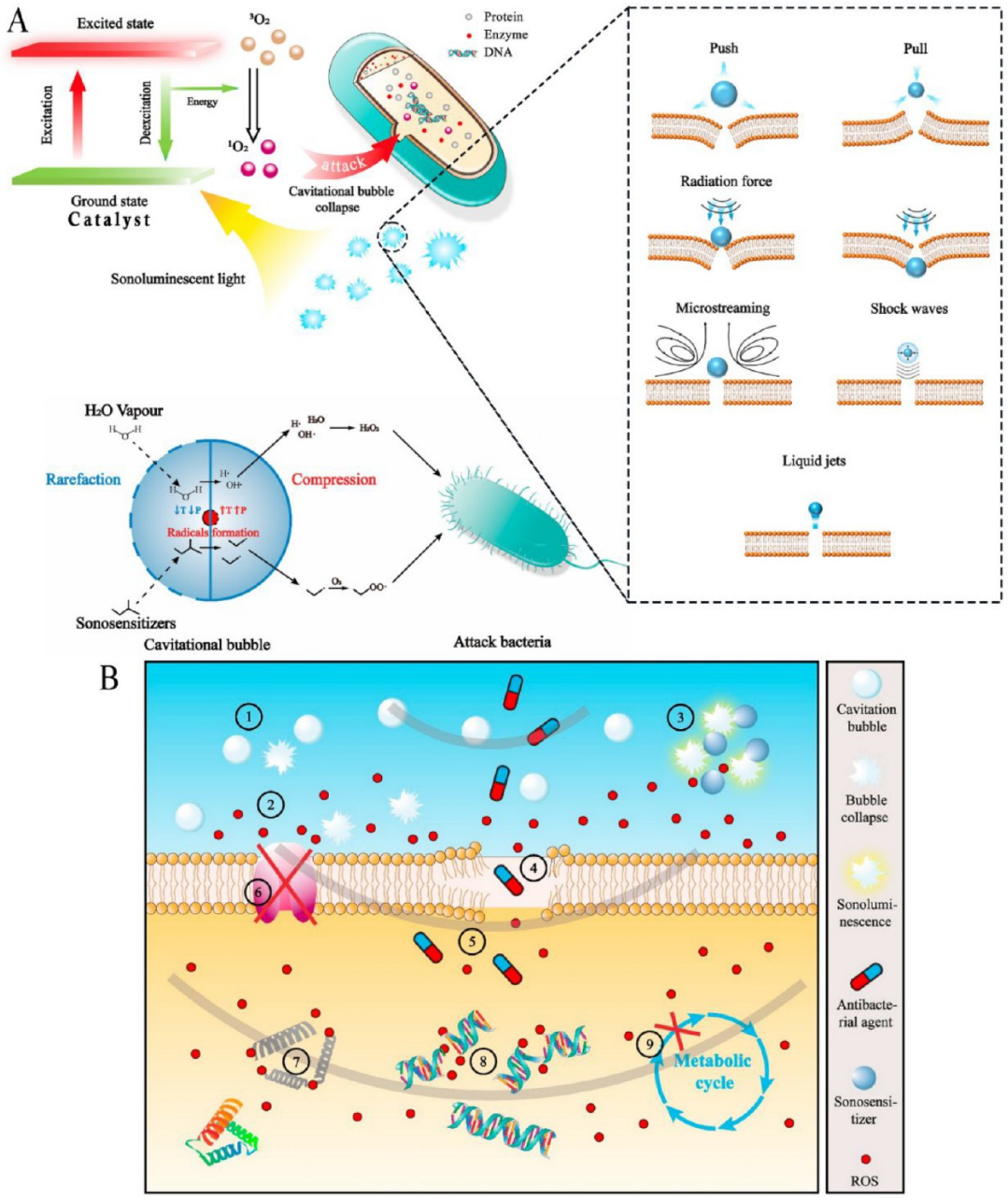

Figure 11. (A) Different types of disinfection mechanisms under the combined effects of ultrasonication and photocatalysis. (B) Schematic mechanisms of disinfection of bacteria and different types of cell membrane perforation caused by acoustic cavitation. The numbers represent the following processes: (1) formation and collapse of cavitation bubbles; (2) production of reactive oxidative species by sonochemistry; (3) reactive species formation by sonoluminescence; (4) membrane perforation; (5) promote penetration of antibacterial agents; (6) transmembrane protein inactivation; (7) intracellular protein and enzyme inactivation; (8) DNA breakage; and (9) metabolism inhibition. Adapted with permission from ref 39. Copyright 2020 Elsevier.

(kW), V is the volume of the reaction solution (L), t represents time (s), and C and C_0 are the concentrations of pollutant at time t and 0, respectively. The 1000 and 60 values are converting constants for kW to W and s to min conversion, respectively. For a pseudo-first reaction model reaction in a batch reactor, the above-mentioned equations can be simplified as it is described in eq 58.[100]

$$E_{EO} = \frac{P_e \times 38.4}{V \times K_{app}} \tag{58}$$

There are plenty of studies that conducted electrical energy consumption analysis for photocatalytic and sonocatalytic degradation systems.[101−103] But, to the best of our knowledge, there are no review studies analyzing the electrical energy consumption of sonophotocatalytic systems. Using experimentally available data from the literature, the electrical energy consumption calculations were carried out for some of previous investigations. Table 1 summarizes key parameters and data, including all energy consumption data translated into cost values. It can be noticed that, in all cases, the E_{EO} of sonophotocatalytic system is lower than the sum of photocatalytic and sonocatalytic systems cost ($E_{EO(UV/US/Cat)}$ <

https://doi.org/10.1021/acsnanoscienceau.2c00058
ACS Nanosci. Au 2023, 3, 103−129

$E_{EO(UV/Cat)}$ + $E_{EO(US/Cat)}$), confirming the efficacy and cost-effectiveness of the integrated system. This reduction in E_{EO} can be attributed to the synergistic effect between these two radical-producing processes, resulting in an increase in the number of degradation events and shortening the reaction time.

Using enhancers could be another cost-effective approach to reduce the overall costs by enhancing process efficiency. Excellent contribution of enhancers in the production of radical species as well as shortening the reaction time outweigh their costs. Asgari et al.[104] performed an economic assessment on the ZnO/persulfate (PS) system for the degradation of AB113 dye through a sonophotocatalytic process. The spherical ZnO nanoparticles with sizes mostly in the range 30−90 nm were synthesized using a sol−gel method. The authors reported that the ZnO/PS/UV/US system exhibited the best removal performance under the optimized conditions, with about 98% degradation rate in 25 min. The economic analysis was performed for UV only, US only, ZnO, PS, and the integrated ZnO/PS/US/UV system. The costs of US and UV systems were calculated using E_{EO} for each process, with values of 214.2 and 43.8 $/m^3, respectively. Also, the removal capacities of ZnO and PS were calculated as the number of milligrams of contaminant removed by one gram of ZnO or PS and were found to be 11.2 and 16.1 mg/g, respectively. According to the amounts of ZnO and PS required, the costs of ZnO and PS for the treatment of 1 m^3 of wastewater containing 200 mg/L AB113 were $1690.5 and $1064, respectively. In the case of integrated system (ZnO/PS/UV/US), the energy cost was $7.1 and material cost were $92.4 and $55.1 for ZnO and PS used, respectively, clearly showing the efficacy of the PS-assisted sonophotocatalytic system.

There are other factors influencing overall costs. For example, sonophotocatalysts can be reused over several cycles, lowering material consumption. The use of natural sunlight irradiation as a reactions' driving force instead of energy-consuming lamps could also be a promising way of reducing costs. Ahmad et al.[18] examined the degradation of RhB using ZnO-decorated multiwall CNTs through photocatalytic, sonocatalytic, and sonophotocatalytic processes. Their sonophotocatalytic reactor consisted of an open 200 mL cylindrical stainless glass vessel, covered with a transparent sheet to avoid evaporation and a 200 W rectangular shaped ultrasonic bath, as the source of US waves, operating in a fixed frequency (35 kHz). The whole setup was exposed to sun light between 10 a.m. and 4 p.m. with an average intensity of 1.213 × 10^5 Lux unit during this period. Relatively lower reaction time and higher reaction rate constant were obtained in the sonophotocatalytic processes, when compared to the individual ones. The use of electricity from renewable resources (i.e., solar cells) is expected to be able to further reduce the operation costs of a sonophotocatalytic system in the future.

6. APPLICATION OF SONOPHOTOCATALYSIS IN BACTERIAL INACTIVATION AND DISINFECTION

We have mainly focused on the application of sonophotocatalysis in the pollutant degradation while describing and discussing various aspects of sonophotocatalysis, such as enhancement strategies, reactors, and energy consumption. In the following, we would like to specifically deal with an important application, bacterial inactivation and disinfection, where sonophotocatalysis also shows a high potential. Recently, semiconductor nanocatalysts have been used to disinfect microbes and Gram-negative bacteria by means of photocatalysis.[110] The combination of ultrasonication and photocatalysis has also become a powerful technique for disinfecting hard-to-kill antibiotic resistant bacteria. Gram-negative bacterial membranes are characterized by an outer membrane that is made up of lipopolysaccharides (LPS), proteins, and phospholipids.[111] Although they possess a thinner peptidoglycan layer compared to Gram-positive bacteria, they are well-equipped to handle a variety of environmental stresses and mechanical loads.[112] It is also worth mentioning that the shape of the bacterium can have a considerable impact on the disinfection effectiveness of the ultrasonic system.[113] Compared to bacilli/rod-shaped bacteria, cocci/spherical bacteria are more resistant to sonication treatment.[114] There are commonly three steps involved in the disinfection of bacteria by sonophotocatalysis. The first stage begins gradually due to the bacteria's resistance to oxidative stress caused by the reactive species. This self-defense mechanism involves an important antioxidant enzyme, named superoxide dismutase (SOD). However, the constant mechanical shear and extended radical species production breaks the bacterial cell membrane and exposes their inner cellular components, causing rapid disinfection (second step). During the final step, the impact of reactive species is diminished due to the presence of intracellular components and cellular debris resulting in a reduced level of disinfection.[115−117]

Figure 11A illustrates different kinds of disinfection mechanisms involved under the combined effects of ultrasonication and photocatalysis. The physical or mechanical consequences of ultrasound cavitation (such as shock waves, shear pressures, microjets) cause the mechanical rupturing of cell membranes and lead to cellular lysis.[43,118] Additionally, a large number of reactive radical species can be produced from both sonocatalytic and photoinduced chemical reactions (photocatalysis). As a result, DNA and intercellular nucleic acids are ejected from the cell due to cytoplasmic material leakage (see Figure 11B). This can be explained by pressure and pressure gradients during the collapse of cavitation bubbles near or inside the cells. It was also reported that a lower frequency acoustic cavitation has greater mechanical effects than chemical effects related to the produced oxidative species.[119] In the following section, we will present three examples of how sonophotocatalysis can be applied to bacterial disinfection and explain how they confirm cell damage and the release of intercellular components caused by sonophotocatalytic disinfection mechanisms.

Mukherjee et al.[120] reported the complete disinfection of the multidrug resistant *Klebsiella pneumonia* bacteria under blue light irradiation from a LED source in combination with low-frequency ultrasonication using CdS nanorods synthesized *via* hydrothermal reaction. The minimum inhibitory concentration (MIC) was defined as the lowest concentration of the nanomaterial to prevent the growth of bacteria.[121] The integrated disinfection technique was able to eradicate 10^6 CFU/mL (CFU: colony-forming units) of Gram-negative *Klebsiella pneumonia* efficiently in 20 min. This bacterium has a peptidoglycan layer containing cross-linked sugar and amino acids and has high permeability, making it easy for nanoparticles and oxidative species to pass through. The cell membrane's LPS and phospholipid bilayer are the main targets of oxidative radical attacks generated by sonophotocatalysis.[122] The mechanism of integrated system in disinfection of *Klebsiella pneumonia* is depicted in Figure 12A. The

https://doi.org/10.1021/acsnanoscienceau.2c00058
ACS Nanosci. Au 2023, 3, 103−129

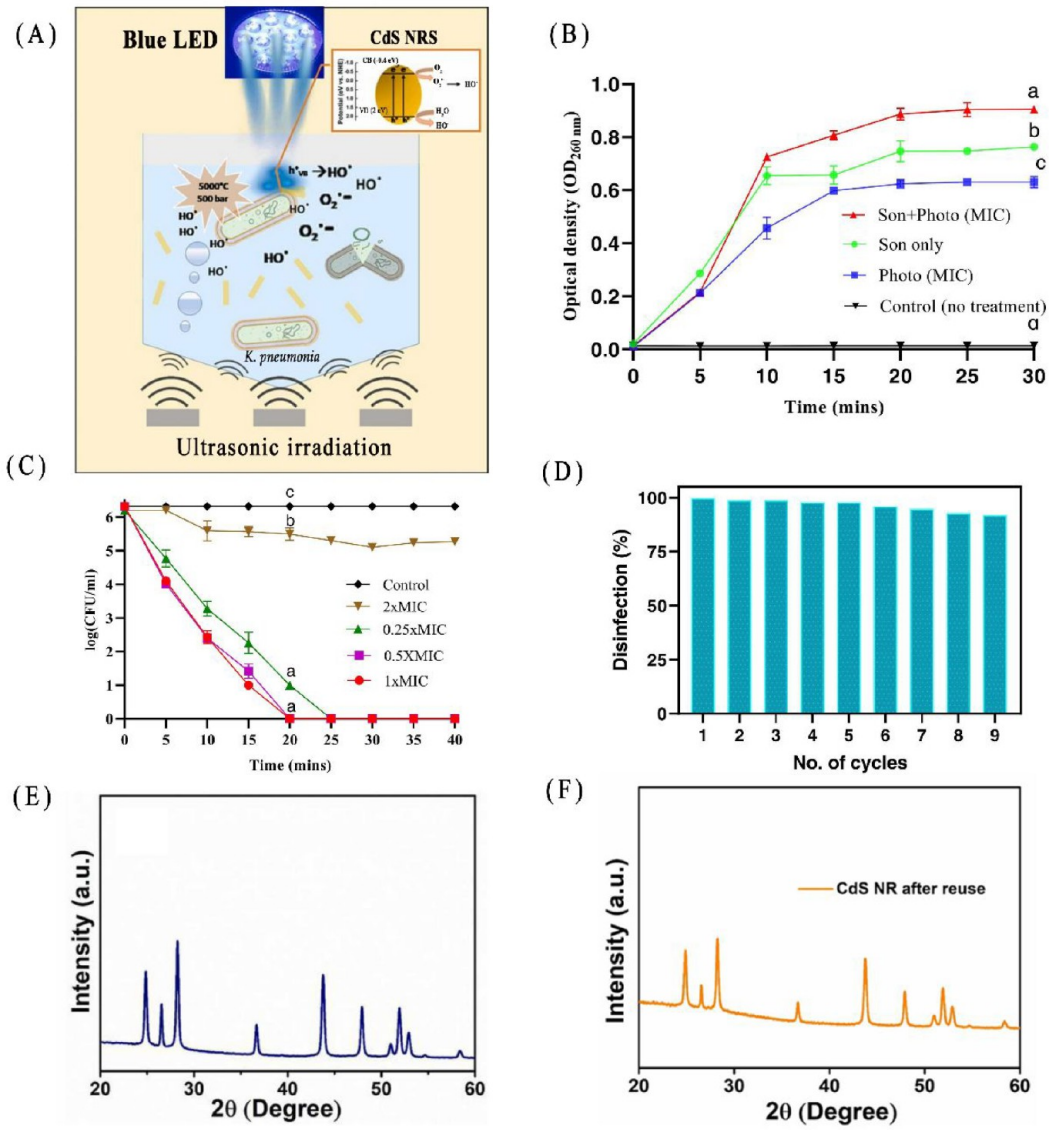

Figure 12. (A) Expulsion of 260 nm absorbing material of *Klebsiella pneumonia* after ultrasonication, photocatalysis, and a combination of ultrasonication and photocatalysis (Son, ultrasonication; photo, photocatalysis (at MIC: 250 mg/L)). (B) Schematic sonophotocatalytic disinfection mechanism of *Klebsiella pneumonia* using CdS nanorods. (C) Effect of catalyst dosage on the sonophotocatalytic disinfection of *Klebsiella pneumonia* (MIC of CdS nanorod, 250 mg/L; light intensity, 15 mW/cm^2). (D) Stability of CdS nanorods after multiple cycles of disinfection. XRD patterns of CdS nanorods (E) before and (F) after cyclic sonophotocatalytic tests. Reproduced with permission from ref 120. Copyright 2022 Elsevier.

effectiveness of ultrasonication-produced shockwaves combined with photocatalysis in disrupting the pathogen's cell membrane was also assessed. These two processes together caused leakage and discharge of compounds, that mainly have absorption around 260 nm, into the supernatant. As seen in Figure 12B, the optical density at 260 nm ($OD_{260\ nm}$) for the separate photocatalytic and ultrasonication systems was significantly higher than the control without any treatment. When the two treatments were combined, the discharge of intracellular components was remarkably larger than when only ultrasonication or photocatalysis was applied. Compared to sonolysis, photocatalysis resulted in a slower rupture of the cell wall and release of intracellular components. Benefiting from the synergy index of 1.817 for sonophotocatalytic process (CdS-1xMIC: 250 mg/L; Figure 12C), the combined technique exhibited complementary and additive efficiency. A similar performance was also achieved using 0.5xMIC CdS nanorods, which successfully managed to reduce the use of the nanomaterial below its MIC by coupling it with sonication (Figure 12C). Thus, the combination of these two processes allowed for the use of nanoparticles at much lower concentrations, which facilitates the practical application of sonophotocatalysis. Also, the electrical energy consumption values were 2.840, 0.8235, and 0.4709 kWh/L for sonolytic, photocatalytic, and sonophotocatalytic (CdS 1xMIC) treatment methods, respectively. The stability test results showed that the catalytic activity of the nanomaterial remained over 92% after nine cycles, confirming the high structural and functional stability of nanocatalysts under disinfection conditions (Figure 12D). As seen in Figure 12E,F, XRD patterns confirmed no significant structural crystalline changes of the CdS nanorods before and after the disinfection reactions, which demonstrates that ultrasonic waves did not damage the catalyst.

https://doi.org/10.1021/acsnanoscienceau.2c00058
ACS Nanosci. Au 2023, 3, 103−129

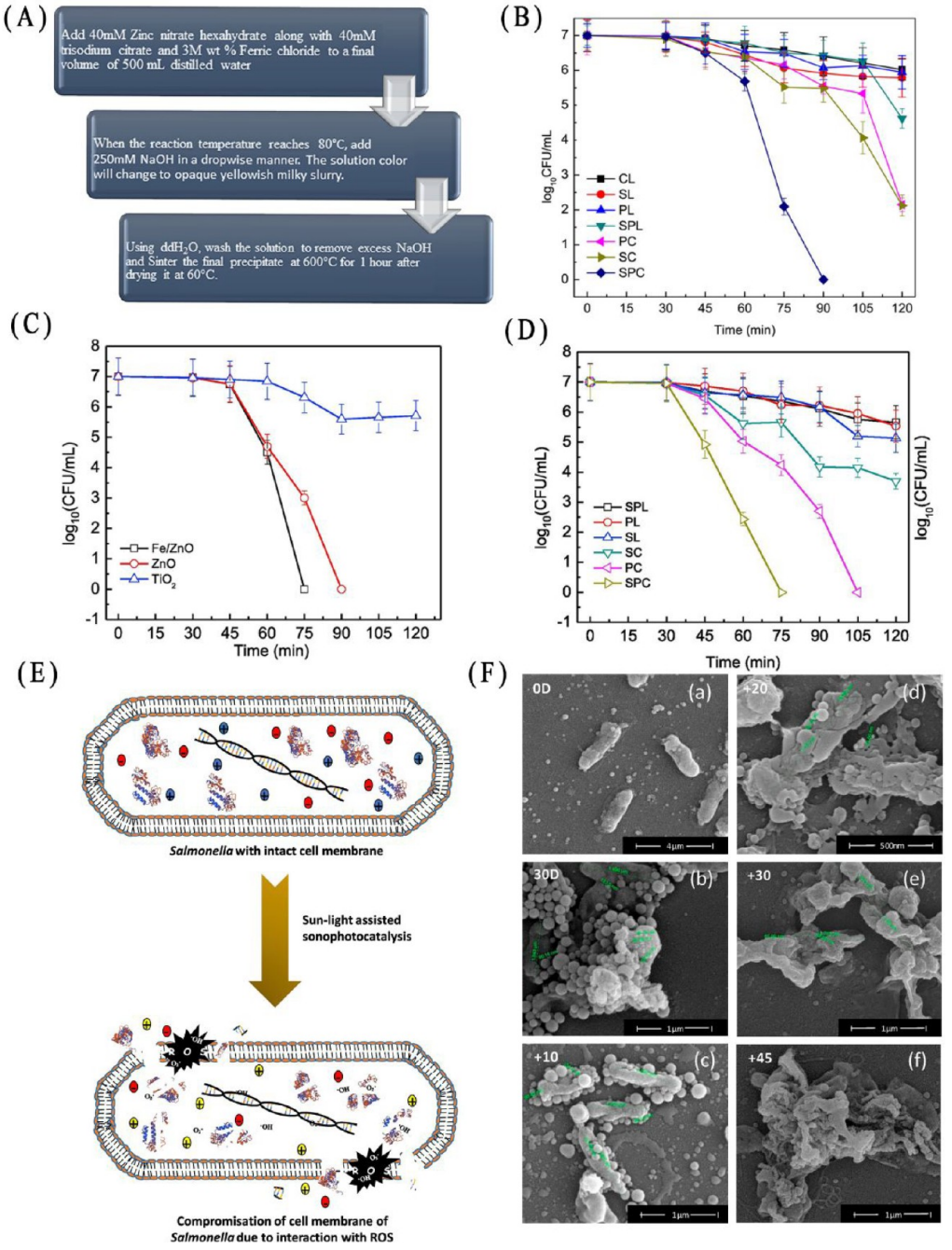

Figure 13. (A) Synthesis flowchart of Fe/ZnO. (B) Different controlled experiments for *Shigella dysenteriae* disinfection (SPC, sonophotocatalysis; SC, sonocatalysis; PC, photocatalysis; SPL, sonophotolysis; PL, photolysis; SL, sonolysis; CL, catalysis). (C) Effect of different catalysts on the solar-sonophotocatalytic activity of *S. typhimurium*. (D) Comparative study and (E) proposed mechanism for sonophotocatalytic disinfection of *S. typhimurium*. (F) (a) and (b) the FESEM images of *S. typhimurium* without the presence of light and ultrasound at t = 0 and t = 30 min, respectively, (c–f) FESEM images of *S. typhimurium* that was subjected to solar-sonophotocatalysis at 10, 20, 30, and 45 min treatment, respectively (ZnO/Fe loading = 200 ppm, bacterial loading ≈10^7 CFU/mL, intensity of sunlight 55,000 lx). (A and B) Reproduced with permission from ref 123. Copyright 2020 Elsevier. (C–F) Reproduced with permission from ref 124. Copyright 2018 Elsevier.

Rahman et al.[123] developed Fe-doped ZnO (Fe/ZnO) nanoparticles for the Vis light-assisted sonophotocatalytic disinfection of *Shigella dysenteriae*. The ZnO nanoparticles were synthesized through colloidal and precipitation routes using zinc nitrate hexahydrate as precursor (Figure 13A). This work compared the effectiveness of sonophotocatalysis, sonocatalysis, and photocatalysis on the removal of the aforementioned bacteria. The results showed in Figure 13B concluded that sonophotocatalysis outperformed any other processes. Excluding the 30 min of initial dark phase, the sonophotocatalysis method achieved a full log reduction of 10^7 CFU/mL *Shigella dysenteriae* in 60 min. In contrast, photocatalysis functioned similarly to sonocatalysis, both of which were unable to entirely disinfect bacteria load even after 1.5 h of reaction, leaving ≈2.1 log CFU/mL bacteria unaffected. However, sonophotocatalysis affected the metabolic processes of *Shigella dysenteriae*. It effectively multiplied reactive species production, primarily containing h^+ and $O_2^{\bullet -}$ radicals, along

https://doi.org/10.1021/acsnanoscienceau.2c00058
ACS Nanosci. Au 2023, 3, 103–129

Table 2. Summary of Sonophotocatalytic Degradation Experiments Reviewed in This Article

Nanocatalyst	Light source	Ultrasonic source	Model pollutant	Reaction time	Catalytic performance	Reference
TiO_2	UV light, 400 W	80 kHz, 120 W	Olive mill wastewater	120 min	100% toxicity removal	45
Sheet-like ZnO	UV light, 300W	40 kHz, 200 W	Methyl orange	100 min	~80%	46
TiO_2/CuO/graphene	UV−C, 80 W	40 kHz, 150 W	Methylene blue	60 min	100%	51
TiO_2/CuO/graphene	Xe lamp, 40 W	40 kHz, 150 W	Methylene blue	80 min	100%	51
$ZnIn_2S_4$ nanostars (NU@ZIS20)	300 W halogen lamp	20 kHz, 200 W	Tetracycline	35 min	99%	52
N, Cu, codoped TiO_2 functionalized CNT	Xe lamp, 200 W	400W	Sulfamethoxazole	60 min	100%	53
Zn−Cu−Mg-mixed metal hydroxide/g-C_3N_4	Visible LED lamp, 15 W	40 kHz, 300 W	Sulfadiazine	200 min	93% COD removal	54
Fe-doped TiO_2	Mercury lamp, 30 W	37 kHz, 100 W	Diazinon	100 min	85%	20
Fe-doped TiO_2, H_2O_2 assisted reaction	UV light, 24 W	50 kHz, 296 W	Paracetamol	30 min	100%	16
Ag-doped *h*-MoO_3 nanorods	Sunlight, 1205 W	100 W	Methylene blue	90 min	98.8%	61
N-doped TiO_2	UV lamp, 300 W	20 kHz, 750 W	4-acetamidophenol	180 min	91%	62
Sm-doped TiO_2	UV lamp, 300 W	20 kHz, 750 W	4-acetamidophenol	180 min	87%	62
N-doped ZnO	N/A	40 kHz, 200 W	Nigrosine	90 min	92%	64
MoS_2/C peroxymonosulfate assisted reaction	Visible light, high-pressure Xe-lamp	40 kHz	Levofloxacin	80 min	100%	19
MgO@CNT	UV lamp, 150 W	24 kHz	Sulfadiazine	80 min	100%	10
MgO@zeolite	UVA, 24 W	24 W/cm^2	Textile wastewater sample	240 min	78% COD removal	66
WO_3/CNT	Visible light, 300 W/m^2	24 kHz	Tetracycline	60 min	100%	71
ZnO/CuO	400 W solar simulator	80 kHz, 60 W	Parathion	60 min	100%	74
$FeVO_4$@BiOCl, H_2O_2 assisted reaction	UV lamp, 8 W	20 kHz, 125 W	*p*-nitrophenol	50 min	100%	75
ZnO/ZnS nanotube	500 W Hg-lamp	N/A	Methylene blue	50 min	63.3%	76
N/Ti^{3+} codoped TiO_2/Bi_2WO_6	500 W xenon lamp	35 kHz, 180 W	Methylene blue	50 min	98%	17
CuO−TiO_2/rGO	UV light	40 kHz	Methyl orange	90 min	99%	83
Fe-doped Bi_2O_3 + Ar bubbling assisted reaction	UV−C lamp, 4 W	37 kHz	Basic brown 1	42 min	99%	85
C−N codoped black TiO_2 H_2O_2 assisted reaction	Visible light, 500 W	30 kHz	Palm oil mill effluent	60 min	75.48%	60
$FeVO_4$@CeO_2 H_2O_2 assisted reaction	UV light	20 kHz, 125 W	4-nitrophenol	30 min	100%	96
ZnO nanoparticle	150 W/m^2	59 kHz	Rhodamine B	10 min	100%	58
Cu_2O/MoS_2/rGO	150 W, halogen lamp	40 kHz, 120 W	Tetracycline	10 min	100%	97
			Ciprofloxacin	75 min	94%	
CeO_2−ZrO_2@MoS_2	Visible light, 250 W	40 and 970 kHz, 0−600 W	Naproxen	40 min	96%	98
CdS nanorods	Blue LED light, 150 W/m^2	700 W	*Klebsiella pneumonia* bacteria	20 min	100% (10^6 CFU/mL)	120
ZnO	Visible light	40 kHz bath sonicator	*Shigella* bacteria	120 min	100% (10^7 CFU/mL)	123
Fe-doped ZnO				90 min	100% (10^7 CFU/mL)	
Fe-doped ZnO	Sun light	40 kHz bath sonicator	*Salmonella* bacteria	90 min	100% (10^7 CFU/mL)	124

with acoustic cavitation. It perturbed the membrane and resulted in internal DNA damage and the release of intracellular components. In a similar study performed also by the same group, Fe-doped ZnO (ZnO/Fe) nanoparticles were utilized in the disinfection of *Salmonella typhimurium* (*S. typhimurium*) by sunlight-assisted sonophotocatalysis.[124] As seen in Figure 13C, the ZnO/Fe nanoparticles presented higher disinfection efficiency compared to bare ZnO nanoparticles for sonophotocatalytic disinfection. Even so, TiO_2 nanoparticles did not yield a complete disinfection when tested under the same conditions. Due to Fe doping, the e^-/h^+ recombination rate in ZnO/Fe was reduced, unlike in ZnO and TiO_2. Further, the transfer of the charges generated as a result of photoexcitation of Fe led to the generation of oxidative radicals. The DNA, protein, and ion leakage assay provided proof that sonophotocatalysis had damaged the cells. The comparative study showed that the order of disinfection efficiencies followed the order of sonophotocatalysis > photocatalysis > sonocatalysis > sonolysis > photolysis> sonophotolysis (see Figure 13D). In the case of sonophotocatalysis, a complete 7 log (CFU/mL) reduction was achieved within only 45 min. The combined effect of sunlight irradiation, ultrasonic waves as well as presence of the catalyst, was proven to reduce the treatment time compared to control experiments. Figure 13E represents the schematic solar-sonophotocatalytic disinfection mechanism of *S. typhimurium* including the cell's membrane rupture and release of intercellular components into the environment. The complete disintegration and collapse of *S. typhimurium* cells during sonophotocatalysis was further confirmed by FESEM images.

https://doi.org/10.1021/acsnanoscienceau.2c00058
ACS Nanosci. Au 2023, 3, 103−129

As seen in Figure 13F, it is quite likely that internal elements including DNA, proteins, and ions have leaked into the environment. All these evidence confirmed the severe damages on the cell membrane of *S. typhimurium* during the sonophotocatalytic disinfection process and the subsequent leakage of chromosomal DNA into the environment.

A summary of sonophotocatalytic degradation experiments is shown in Table 2, including all the pertinent studies published to date. For better comparison among the examples, important parameters such as catalysts, light sources, ultrasonic sources, model pollutants, reaction time, and degradation efficiencies are provided in this table.

CONCLUSIONS AND PERSPECTIVES

Employing nanocatalyst-based sonophotocatalysis for wastewater treatment and bacterial inactivation and disinfection requires a thorough multidisciplinary (chemical, physical, and engineering) understanding of liquid, solid, and interfacial properties as well as ultrasound parameters. Several chemical and physical events such as radical-producing reactions, cavitations, SL, increased mass transport, surface cleaning, and surface adsorption capacity variation are likely to happen simultaneously and result in considerable improvement in the efficiency. Hence, main limitations of photocatalytic process can possibly be eliminated when using sonophotocatalysis for degradation and disinfection processes (such as resistance in mass transfer and catalyst fouling) without having any significant impact on the structure, crystallinity, or morphology of the nanocatalyst. It is also important to mention that the efficient design of sonophotocatalytic reactors is essential to maintain high efficiency and provide a flexible, sustainable, and cost-effective alternative to conventional photocatalytic and sonocatalytic treatment methods. The sonophotocatalytic system activity can be enhanced by means of nanocatalyst modification techniques (incorporating dopants, using nanosubstrates, and forming efficient heterojunctions) aimed at improving mainly light absorption, optimizing charge transfer pathways, and reducing e^-/h^+ recombination rates. Furthermore, process modification techniques primarily influence sonocatalytic mechanisms such as the nucleation and formation and collapse of cavitation bubbles, and promote the proliferation of radical species in the environment. Acoustic cavitations coupled with photocatalysis showed excellent synergism, affecting energy consumption of the integrated system. Sonophotocatalysis allows researchers to find new ways to improve the efficiency of ultrasound or even search for new strategies to generate cavitation that could be more efficient and of lower treatment costs (for example, by using renewable electricity) in the future.

Due to the lack of standardized data, the presence of various contaminants, and the different operational parameters of each experiment, it is not always possible to reach straightforward conclusions relating nanomaterial's morphology to sonophotocatalytic activity. However, looking at some of the examples described in this manuscript, we will give the reader some insights to help to better rationally design novel nanomaterials, heterojunctions, and composites in the future. Sheet-like and flower-like morphologies usually have higher sonophotocatalytic activity, such as for the case of ZnO nanocatalysts, when compared to rod-like ZnO in the degradation of methyl orange.[46] Furthermore, desert rose morphology of ZnO with 50 nm nanosheet petals outperformed other ZnO morphologies, such as nanospheres, nanowires, and microwires in the RhB sonophotocatalytic removal.[58] For the degradation of MB, ZnS/ZnO nanotubes showed greater degradation rate than their nanorods counterpait.[76] Looking at these examples, we can conclude that nanosheets and nanotubes usually outperformed other nanostructures. In general, nanomaterials possess high specific surface areas, high porosity, and optimal interfacial charge transfer. Low-dimensional nanoscaled materials (2D, 1D, 0D) exhibit a more uniform size distribution compared to bulk materials, allowing for better control of their properties. Their larger surface area allows them to come into contact with a greater portion of photons and pollutants in the solution. Additionally, the energy levels of nanomaterials can also be tuned by modifying their size, doping and creating defects.[125] In particular, 2D nanomaterials benefit from having a high surface area and the possibility of being host materials to form heterojunctions and composites and thereby improved charge transfer.[126,127] Furthermore, in some cases, the charge transfer is favored in one specific direction due to the orientation of the nanostructures such as nanotubes, thereby reducing charge recombination,[128,129] as it could be seen in the previous ZnS/ZnO example. Additionally, nanotubes are generally preferred to nanorods due to their increased surface area with more exposed catalytic active sites to light and adsorbed molecules, with their tendency to form a packed interconnected network and reduced charge recombination rate.[130]

There are several factors that must be considered for future investigations in order to improve its efficiency and extend its application to other fields:

- The simultaneous degradation of multiple contaminants should be investigated. Contrary to the cases reported in most articles, where artificial wastewaters only contain a single contaminant, real effluents always include more than one type of contaminants. The performance of sonophotocatalysis through degradation of multiple contaminants must be explored, as well as possible new phenomena, extra synergism, or better removal capability of semiconductors. To really assess the efficiency of sonophotocatalysis and promote its practical application, the analysis of real wastewater samples should be performed.
- It is highly needed to standardize the experimental conditions and characterization tests in the field of sonophotocatalysis if we want to fairly compare different materials. Since a broad range of catalysts, pollutants, catalyst dosages, pollutant concentrations, reaction times, light and US power sources, and different reactor sizes have been employed in the literature, progress cannot be assessed in a rational way. For example, a specific dye or pollutant can be selected as standard contaminant for future investigations. Also, reaction kinetic constants must always be provided for all processes and controlled experiments. With all these, researchers in this field will be able to compare the catalyst activities and rationally design new nanomaterials and heterojunction-enhanced nanocatalysts.
- Deeper study of mechanisms and pathways is of high necessity. Because of the short time interval in which the sonophotocatalytic reaction pathways take place, deeper mechanism and pathway analysis are hard but necessary. Future research could also focus on exploring possible effects of ultrasound on nanomaterial properties (such as

https://doi.org/10.1021/acsnanoscienceau.2c00058
ACS Nanosci. Au 2023, 3, 103−129

band structure and Fermi energy) and its impacts on the thermodynamics and kinetics of reactions. Sonophotocatalytic disinfection of bacteria is also not understood to its full extent. Particularly, a systematic investigation is needed to understand how sonophotocatalysis differs from other oxidation processes in terms of disinfection pathways at the molecular level. Along with theoretical simulations, *in situ* characterization techniques (e.g., *in situ* FTIR, *in situ* Raman) are promising tools in achieving this goal.

- Fabricating integrated Z-scheme sonophotocatalytic systems requires further research and should be one of the main focuses of future research to promote the optimization of redox and oxidation potentials in sonophotocatalysts and boost the degradation efficiency in such systems.
- Precise investigation of attenuation of photons and US in large-scale usage should be taken into consideration. Although there are a lot of studies concerning sonophotocatalytic degradation of pollutants in at the laboratory scale, little is known about reactor parameters optimization, the effective penetration distance of photons and US at the larger scale. Attenuation of ultrasonic waves and light irradiation caused by various parameters such as solvent and dissolved organics and catalyst particles is one of the fundamental phenomena that must be taken into consideration in order to bring this technique into large-scale applications.
- The stability of nanomaterials is related to several factors. One of them is correlated with their stability in acid or basic media. Additionally, their stability under light (especially UV light) and ultrasonic waves needs also to be considered and studied. Sonophotocatalysis should not damage the catalyst's physical and/or chemical structure to avoid its structural or morphological changes. Also, in the case of binary or ternary composites, ultrasonic waves should not adversely affect their integrity. To achieve this goal, rational morphology design (e.g., core@shell structures) or formation of strong covalent bonds instead of simple van der Waals interactions among the nanocomponents can be used to strengthen their junctions and interfaces.[131] Performing leaching tests, TEM, XRD, and FTIR analysis before and after the experiments is highly recommended for future investigations to study the integrity and structural and morphological features of the fabricated nanocatalysts.
- A more in-depth economic assessment will be required to use this technique for scale-up processes. Electrical energy consumption accounts for part of the sonophotocatalytic degradation of wastewaters. Other expenses (such as costs of reactors, piping, valves, site work, engineering, part replacement, labor, chemicals, characterizations, sampling, operation, and maintenance) need to be considered and optimized to lowest without compromising the performance.
- The majority of published articles on sonophotocatalysis employed UV-active materials. Other photocatalysts with absorption in the Vis and NIR regions of the spectra should be considered to increase the sunlight and SL utilization and the overall efficacy of sonophotocatalysis.
- In this interdisciplinary field, computational modeling/calculations are necessary to support all critical elements and operational parameters such as the design of catalysts, reactors, etc.
- "Self propelled nanorobotics are holding outstanding applications in biosensing, biomedicine, environment, and chemistry fields, which is a new application of cutting-edge multidisciplinary field in nanotechnology.[132−135] Catalytic micro/nano robots are nanomaterials that can effectively convert external forces such as magnetic field, light source (photocatalytic), ultrasonic waves (sonocatalytic), and chemical fuels to mechanical motion for desired applications. For example, Ussia et al.[133] used self propelled black titania/silver nanorobots under light irradiation for treatment of bacterial biofilm. The molecular motion of light propelled micro/nano motors could be controlled by adjusting the light intensity. Photocatalytic nanorobots could give rise to the concentration of reactive oxygen species that affectively degrade bacteria.[132,133] Also, it has been reported that ultrasonic waves can increase the motion of micromotors due to the production of microbubbles.[135] As a new subject, the simultaneous usage of light and ultrasonic sources as driving forces could be investigated in the future to improve the performance of nanomaterial for micro/nano robot preparation for biomedical applications.

Overall, due to the combination of physical, sonochemical, and photochemical processes, sonophotocatalysis has indisputable advantages over classic photocatalysis, allowing for researchers to build enhanced systems with larger degradation potentials. We hope that we have been able to grant a comprehensive overview of the research progress in this area and shed some light on the advantages, its limitations, and future directions to promote its use in general, and ultimately, in industrial applications.

AUTHOR INFORMATION

Corresponding Authors

Cristina Rodriguez-Seco − *Institut National de la Recherche Scientifique (INRS)-Centre Énergie Materiaux et Télécommunications, Varennes J3X 1P7 Québec, Canada*; Email: Cristina.rodriguez.seco@inrs.ca

Dongling Ma − *Institut National de la Recherche Scientifique (INRS)-Centre Énergie Materiaux et Télécommunications, Varennes J3X 1P7 Québec, Canada*; orcid.org/0000-0001-8558-3150; Email: Dongling.ma@inrs.ca

Authors

Sina Moradi − *Institut National de la Recherche Scientifique (INRS)-Centre Énergie Materiaux et Télécommunications, Varennes J3X 1P7 Québec, Canada*

Farzan Hayati − *Department of Chemical and Biological Engineering, University of Saskatchewan, Saskatoon S7N 5A9 SK, Canada*

Complete contact information is available at: https://pubs.acs.org/10.1021/acsnanoscienceau.2c00058

Author Contributions

All the authors have accepted responsibility for the entire content of this submitted manuscript and approved submission.

https://doi.org/10.1021/acsnanoscienceau.2c00058
ACS Nanosci. Au 2023, 3, 103−129

Funding

The authors greatly appreciate the financial support from the Natural Sciences and Engineering Research Council of Canada (NSERC), RGPIN-2020-05921, the Banting Postdoctoral Fellowship program, and the Dean's Scholarship (F.H.).

Notes

The authors declare no competing financial interest.

■ ACKNOWLEDGMENTS

D.M. is grateful to the Canada Research Chairs program and the Natural Sciences and Engineering Research Council of Canada (NSERC) program of Canada. C.R.S. is grateful to NSERC for Postdoctoral Banting Fellowship. Additionally, the authors would like to extend their thanks to the College of Graduate and Postdoctoral Studies, the University of Saskatchewan, for the financial support in the form of a Dean's Scholarship (F.H.).

■ REFERENCES

(1) Vasilachi, I. C.; Asiminicesei, D. M.; Fertu, D. I.; Gavrilescu, M. Occurrence and Fate of Emerging Pollutants in Water Environment and Options for Their Removal. *Water* **2021**, *13* (2), 181.

(2) Michael, I.; Rizzo, L.; McArdell, C. S.; Manaia, C. M.; Merlin, C.; Schwartz, T.; Dagot, C.; Fatta-Kassinos, D. Urban Wastewater Treatment Plants as Hotspots for the Release of Antibiotics in the Environment: A Review. *Water Res.* **2013**, *47* (3), 957−995.

(3) Demirbas, A. Agricultural Based Activated Carbons for the Removal of Dyes from Aqueous Solutions: A Review. *J. Hazard. Mater.* **2009**, *167* (1−3), 1−9.

(4) Moradi, S.; Isari, A. A.; Hayati, F.; Rezaei Kalantary, R.; Kakavandi, B. Co-Implanting of TiO_2 and Liquid-Phase-Delaminated g-C_3N_4 on Multi-Functional Graphene Nanobridges for Enhancing Photocatalytic Degradation of Acetaminophen. *Chem. Eng. J.* **2021**, *414*, 128618.

(5) Ye, Z.; Kong, L.; Chen, F.; Chen, Z.; Lin, Y.; Liu, C. A Comparative Study of Photocatalytic Activity of ZnS Photocatalyst for Degradation of Various Dyes. *Optik (Stuttg).* **2018**, *164*, 345−354.

(6) Fu, J.; Yu, J.; Jiang, C.; Cheng, B. g-C_3N_4-Based Heterostructured Photocatalysts. *Adv. Energy Mater.* **2018**, *8* (3), 1701503.

(7) Chen, D.; Cheng, Y.; Zhou, N.; Chen, P.; Wang, Y.; Li, K.; Huo, S.; Cheng, P.; Peng, P.; Zhang, R.; Wang, L.; Liu, H.; Liu, Y.; Ruan, R. Photocatalytic Degradation of Organic Pollutants Using TiO_2-Based Photocatalysts: A Review. *J. Clean. Prod.* **2020**, *268*, 121725.

(8) Serrà, A.; Pip, P.; Gómez, E.; Philippe, L. Efficient Magnetic Hybrid ZnO-Based Photocatalysts for Visible-Light-Driven Removal of Toxic Cyanobacteria Blooms and Cyanotoxins. *Appl. Catal., B* **2020**, *268*, 118745.

(9) Ruan, S.; Huang, W.; Zhao, M.; Song, H.; Gao, Z. A Z-Scheme Mechanism of the Novel ZnO/CuO n-n Heterojunction for Photocatalytic Degradation of Acid Orange 7. *Mater. Sci. Semicond. Process.* **2020**, *107*, 104835.

(10) Hayati, F.; Isari, A. A.; Anvaripour, B.; Fattahi, M.; Kakavandi, B. Ultrasound-Assisted Photocatalytic Degradation of Sulfadiazine Using MgO@CNT Heterojunction Composite: Effective Factors, Pathway and Biodegradability Studies. *Chem. Eng. J.* **2020**, *381*, 122636.

(11) Yousef Tizhoosh, N.; Khataee, A.; Hassandoost, R.; Darvishi Cheshmeh Soltani, R.; Doustkhah, E. Ultrasound-Engineered Synthesis of WS2@CeO_2 Heterostructure for Sonocatalytic Degradation of Tylosin. *Ultrason. Sonochem.* **2020**, *67* (March), 105114.

(12) Sadeghi Rad, T.; Ansarian, Z.; Khataee, A.; Vahid, B.; Doustkhah, E. N-Doped Graphitic Carbon as a Nanoporous MOF-Derived Nanoarchitecture for the Efficient Sonocatalytic Degradation Process. *Sep. Purif. Technol.* **2021**, *256*, 117811.

(13) Kakavandi, B.; Bahari, N.; Rezaei Kalantary, R.; Dehghani Fard, E. Enhanced Sono-Photocatalysis of Tetracycline Antibiotic Using TiO_2 Decorated on Magnetic Activated Carbon (MAC@T) Coupled with US and UV: A New Hybrid System. *Ultrason. Sonochem.* **2019**, *55*, 75−85.

(14) Taghipour, T.; Karimipour, G. R.; Ghaedi, M.; Rahimi, M. R.; Mosleh, S. Sonophotocatalytic Treatment of Diazinon Using Visible Light-Driven Ce:Cu-1,4-BDOAH2 Photocatalyst in a Batch-Mode Process: Response Surface Methodology and Optimization. *Appl. Organomet. Chem.* **2018**, *32* (1), e3962.

(15) Abdurahman, M. H.; Abdullah, A. Z.; Shoparwe, N. F. A Comprehensive Review on Sonocatalytic, Photocatalytic, and Sonophotocatalytic Processes for the Degradation of Antibiotics in Water: Synergistic Mechanism and Degradation Pathway. *Chem. Eng. J.* **2021**, *413*, 127412.

(16) Yap, H. C.; Pang, Y. L.; Lim, S.; Lai, C. W.; Abdullah, A. Z. Enhanced Sonophotocatalytic Degradation of Paracetamol in the Presence of Fe-Doped TiO_2 Nanoparticles and H_2O_2. *Environ. Earth Sci.* **2020**, *79* (19), 1−12.

(17) Sun, M.; Yao, Y.; Ding, W.; Anandan, S. N/Ti3+ Co-Doping Biphasic TiO_2/Bi_2WO_6 Heterojunctions: Hydrothermal Fabrication and Sonophotocatalytic Degradation of Organic Pollutants. *J. Alloys Compd.* **2020**, *820*, 153172.

(18) Ahmad, M.; Ahmed, E.; Hong, Z. L.; Ahmed, W.; Elhissi, A.; Khalid, N. R. Photocatalytic, Sonocatalytic and Sonophotocatalytic Degradation of Rhodamine B Using ZnO/CNTs Composites Photocatalysts. *Ultrason. Sonochem.* **2014**, *21* (2), 761−773.

(19) Zeng, L.; Li, S.; Li, X.; Li, J.; Fan, S.; Chen, X.; Yin, Z.; Tadé, M.; Liu, S. Visible-Light-Driven Sonophotocatalysis and Peroxymonosulfate Activation over 3D Urchin-like MoS_2/C Nanoparticles for Accelerating Levofloxacin Elimination: Optimization and Kinetic Study. *Chem. Eng. J.* **2019**, *378* (June), 122039.

(20) Tabasideh, S.; Maleki, A.; Shahmoradi, B.; Ghahremani, E.; McKay, G. Sonophotocatalytic Degradation of Diazinon in Aqueous Solution Using Iron-Doped TiO_2 Nanoparticles. *Sep. Purif. Technol.* **2017**, *189* (April), 186−192.

(21) Yang, H.; He, D.; Liu, C.; Zhang, T.; Qu, J.; Jin, D.; Zhang, K.; Lv, Y.; Zhang, Z.; Zhang, Y. Chemosphere Visible-Light-Driven Photocatalytic Disinfection by S-Scheme α-Fe_2O_3/g-C_3N_4 Heterojunction : Bactericidal Performance and Mechanism Insight. *Chemosphere* **2022**, *287* (P1), 132072.

(22) Das, S.; Sinha, S.; Suar, M.; Yun, S. Il; Mishra, A.; Tripathy, S. K. Solar-Photocatalytic Disinfection of Vibrio Cholerae by Using Ag@ZnO Core-Shell Structure Nanocomposites. *J. Photochem. Photobiol. B Biol.* **2015**, *142*, 68−76.

(23) Matafonova, G.; Batoev, V. Review on Low- and High-Frequency Sonolytic, Sonophotolytic and Sonophotochemical Processes for Inactivating Pathogenic Microorganisms in Aqueous Media. *Water Res.* **2019**, *166*, 115085.

(24) Drosou, C.; Coz, A.; Xekoukoulotakis, N. P.; Moya, A.; Vergara, Y.; Mantzavinos, D. Peracetic Acid-Enhanced Photocatalytic and Sonophotocatalytic Inactivation of E. Coli in Aqueous Suspensions. *J. Chem. Technol. Biotechnol.* **2010**, *85* (8), 1049−1053.

(25) Yusof, N. S. M.; Babgi, B.; Alghamdi, Y.; Aksu, M.; Madhavan, J.; Ashokkumar, M. Physical and Chemical Effects of Acoustic Cavitation in Selected Ultrasonic Cleaning Applications. *Ultrason. Sonochem.* **2016**, *29*, 568−576.

(26) Dehghan, S.; Kakavandi, B.; Kalantary, R. R. Heterogeneous Sonocatalytic Degradation of Amoxicillin Using ZnO@Fe_3O_4Magnetic Nanocomposite: Influential Factors, Reusability and Mechanisms. *J. Mol. Liq.* **2018**, *264*, 98−109.

(27) Moradi, S.; Sobhgol, S. A.; Hayati, F.; Isari, A. A.; Kakavandi, B.; Bashardoust, P.; Anvaripour, B. Performance and Reaction Mechanism of MgO/ZnO/Graphene Ternary Nanocomposite in Coupling with LED and Ultrasound Waves for the Degradation of Sulfamethoxazole and Pharmaceutical Wastewater. *Sep. Purif. Technol.* **2020**, *251* (May), 117373.

(28) Karim, A. V.; Shriwastav, A. Degradation of Cipro Fl Oxacin Using Photo, Sono, and Sonophotocatalytic Oxidation with Visible Light and Low-Frequency Ultrasound : Degradation Kinetics and Pathways. *Chem. Eng. J.* **2020**, *392*, 124853.

(29) Joseph, C. G.; Li Puma, G.; Bono, A.; Krishnaiah, D. Sonophotocatalysis in Advanced Oxidation Process: A Short Review. *Ultrason. Sonochem.* **2009**, *16* (5), 583−589.
(30) Authier, O.; Ouhabaz, H.; Bedogni, S. Modeling of Sonochemistry in Water in the Presence of Dissolved Carbon Dioxide. *Ultrason. Sonochem.* **2018**, *45*, 17−28.
(31) Ji, R.; Pflieger, R.; Virot, M.; Nikitenko, S. I. Multibubble Sonochemistry and Sonoluminescence at 100 kHz: The Missing Link between Low- and High-Frequency Ultrasound. *J. Phys. Chem. B* **2018**, *122* (27), 6989−6994.
(32) Ogi, H.; Hirao, M.; Shimoyama, M. Activation of TiO_2 Photocatalyst by Single-Bubble Sonoluminescence for Water Treatment. *Ultrasonics* **2002**, *40* (1−8), 649−650.
(33) Shimizu, N.; Ogino, C.; Dadjour, M. F.; Murata, T. Sonocatalytic Degradation of Methylene Blue with TiO_2 Pellets in Water. *Ultrason. Sonochem.* **2007**, *14* (2), 184−190.
(34) Balaji, C.; Moholkar, V. S.; Pandit, A. B.; Ashokkumar, M. Mechanistic Investigations on Sonophotocatalytic Degradation of Textile Dyes with Surface Active Solutes. *Ind. Eng. Chem. Res.* **2011**, *50* (20), 11485−11494.
(35) Qiu, P.; Park, B.; Choi, J.; Thokchom, B.; Pandit, A. B.; Khim, J. A Review on Heterogeneous Sonocatalyst for Treatment of Organic Pollutants in Aqueous Phase Based on Catalytic Mechanism. *Ultrason. Sonochem.* **2018**, *45*, 29−49.
(36) Choi, Y.; Lee, D.; Hong, S.; Khan, S.; Darya, B.; Lee, J. Y.; Chung, J.; Cho, S. H. Investigation of the Synergistic Effect of Sonolysis and Photocatalysis of Titanium Dioxide for Organic Dye Degradation. *Catalysts* **2020**, *10* (5), 500.
(37) Li, X.; Wang, W.; Dong, F.; Zhang, Z.; Han, L.; Luo, X.; Huang, J.; Feng, Z.; Chen, Z.; Jia, G.; Zhang, T. Recent Advances in Noncontact External-Field-Assisted Photocatalysis: From Fundamentals to Applications. *ACS Catal.* **2021**, *11* (8), 4739−4769.
(38) Yap, H. C.; Pang, Y. L.; Lim, S.; Abdullah, A. Z.; Ong, H. C.; Wu, C. H. A Comprehensive Review on State-of-the-Art Photo-, Sono-, and Sonophotocatalytic Treatments to Degrade Emerging Contaminants. *Int. J. Environ. Sci. Technol.* **2019**, *16* (1), 601−628.
(39) Dai, J.; Bai, M.; Li, C.; Cui, H.; Lin, L. Advances in the Mechanism of Different Antibacterial Strategies Based on Ultrasound Technique for Controlling Bacterial Contamination in Food Industry. *Trends Food Sci. Technol.* **2020**, *105*, 211−222.
(40) Panda, D.; Manickam, S. Recent Advancements in the Sonophotocatalysis (SPC) and Doped-Sonophotocatalysis (DSPC) for the Treatment of Recalcitrant Hazardous Organic Water Pollutants. *Ultrason. Sonochem.* **2017**, *36*, 481−496.
(41) Disselkamp, R. S.; Judd, K. M.; Hart, T. R.; Peden, C. H. F.; Posakony, G. J.; Bond, L. J. A Comparison between Conventional and Ultrasound-Mediated Heterogeneous Catalysis: Hydrogenation of 3-Buten-1-Ol Aqueous Solutions. *J. Catal.* **2004**, *221* (2), 347−353.
(42) Carcenac, Y.; Tordeux, M.; Wakselman, C.; Diter, P. Convenient Synthesis of Fluorinated Alkanes and Cycloalkanes by Hydrogenation of Perfluoroalkylalkenes under Ultrasound Irradiation. *J. Fluor. Chem.* **2005**, *126* (9−10), 1347−1355.
(43) Mason, T. J.; Cobley, A. J.; Graves, J. E.; Morgan, D. New Evidence for the Inverse Dependence of Mechanical and Chemical Effects on the Frequency of Ultrasound. *Ultrason. Sonochem.* **2011**, *18* (1), 226−230.
(44) Amaniampong, P. N.; Jérôme, F. Catalysis under Ultrasonic Irradiation: A Sound Synergy. *Curr. Opin. Green Sustain. Chem.* **2020**, *22*, 7−12.
(45) Silva, A. M. T.; Nouli, E.; Carmo-Apolinário, Â. C.; Xekoukoulotakis, N. P.; Mantzavinos, D. Sonophotocatalytic/H_2O_2 degradation of Phenolic Compounds in Agro-Industrial Effluents. *Catal. Today* **2007**, *124* (3−4), 232−239.
(46) Yang, R.; Wu, Z.; Yang, Y.; Li, Y.; Zhang, L.; Yu, B. Journal of the Taiwan Institute of Chemical Engineers Understanding the Origin of Synergistic Catalytic Activities for ZnO Based Sonophotocatalytic Degradation of Methyl Orange. *J. Taiwan Inst. Chem. Eng.* **2021**, *119*, 128−135.
(47) Hayati, F.; Moradi, S.; Farshineh, S.; Madani, Z.; Giannakis, S.; Akbar, A.; Kakavandi, B. A Novel, Z-Scheme ZnO@AC@FeO Photocatalyst, Suitable for the Intensification of Photo-Mediated Peroxymonosulfate Activation : Performance, Reactivity and Bisphenol A Degradation Pathways. *J. Environ. Manage.* **2022**, *321*, 115851.
(48) Moradi, S.; Sobhgol, S. A.; Hayati, F.; Isari, A. A.; Kakavandi, B.; Bashardoust, P.; Anvaripour, B. Performance and Reaction Mechanism of MgO/ZnO/Graphene Ternary Nanocomposite in Coupling with LED and Ultrasound Waves for the Degradation of Sulfamethoxazole and Pharmaceutical Wastewater. *Sep. Purif. Technol.* **2020**, *251*, 117373.
(49) Niu, P.; Wu, G.; Chen, P.; Zheng, H.; Cao, Q.; Jiang, H. Optimization of Boron Doped TiO_2 as an Efficient Visible Light-Driven Photocatalyst for Organic Dye Degradation With High Reusability. *Front. Chem.* **2020**, *8* (March), 1−8.
(50) Sharma, S.; Basu, S. Highly Reusable Visible Light Active Hierarchical Porous WO_3/SiO_2 Monolith in Centimeter Length Scale for Enhanced Photocatalytic Degradation of Toxic Pollutants. *Sep. Purif. Technol.* **2020**, *231*, 115916.
(51) Taufik, A.; Muzakki, A.; Saleh, R. Effect of Nanographene Platelets on Adsorption and Sonophotocatalytic Performances of TiO_2/CuO Composite for Removal of Organic Pollutants. *Mater. Res. Bull.* **2018**, *99*, 109−123.
(52) Abazari, R.; Sanati, S.; Morsali, A.; Kirillov, A. M. Instantaneous Sonophotocatalytic Degradation of Tetracycline over NU-1000@$ZnIn_2S_4$ Core-Shell Nanorods as a Robust and Eco-Friendly Catalyst. *Inorg. Chem.* **2021**, *60* (13), 9660−9672.
(53) Isari, A. A.; Hayati, F.; Kakavandi, B.; Rostami, M.; Motevassel, M.; Dehghanifard, E. N, Cu Co-Doped TiO_2@functionalized SWCNT Photocatalyst Coupled with Ultrasound and UV Waves: An Effective Sono-Photocatalysis Process for Pharmaceutical Wastewaters Treatment. *Chem. Eng. J.* **2020**, *392*, 123685.
(54) Gholami, P.; Khataee, A.; Vahid, B.; Karimi, A.; Golizadeh, M.; Ritala, M. Sonophotocatalytic Degradation of Sulfadiazine by Integration of Microfibrillated Carboxymethyl Cellulose with Zn-Cu-Mg Mixed Metal Hydroxide/g-C_3N_4 Composite. *Sep. Purif. Technol.* **2020**, *245* (April), 116866.
(55) Lu, L.; Kobayashi, A.; Tawa, K.; Ozaki, Y. Silver Nanoplates with Special Shapes: Controlled Synthesis and Their Surface Plasmon Resonance and Surface-Enhanced Raman Scattering Properties. *Chem. Mater.* **2006**, *18* (20), 4894−4901.
(56) Zhang, L.; Xu, T.; Zhao, X.; Zhu, Y. Controllable Synthesis of Bi_2MoO_6 and Effect of Morphology and Variation in Local Structure on Photocatalytic Activities. *Appl. Catal., B.* **2010**, *98* (3−4), 138−146.
(57) Zhang, L.; Li, J.; Chen, Z.; Tang, Y.; Yu, Y. Preparation of Fenton Reagent with H_2O_2 Generated by Solar Light-Illuminated Nano-Cu_2O/MWNTs Composites. *Appl. Catal., A.* **2006**, *299* (1−2), 292−297.
(58) Lops, C.; Ancona, A.; Di Cesare, K.; Dumontel, B.; Garino, N.; Canavese, G.; Hérnandez, S.; Cauda, V. Sonophotocatalytic Degradation Mechanisms of Rhodamine B Dye via Radicals Generation by Micro- and Nano-Particles of ZnO. *Appl. Catal., B* **2019**, *243*, 629−640.
(59) Chakma, S.; Moholkar, V. S. Investigation in Mechanistic Issues of Sonocatalysis and Sonophotocatalysis Using Pure and Doped Photocatalysts. *Ultrason. Sonochem.* **2015**, *22*, 287−299.
(60) Rahman, S.; Nawaz, R.; Khan, J. A.; Ullah, H.; Irfan, M.; Glowacz, A.; Lyp-Wronska, K.; Wzorek, L.; Khan, M. K. A.; Jalalah, M.; Alsaiari, M. A.; Almawgani, A. H. Synthesis and Characterization of Carbon and Carbon-Nitrogen Doped Black TiO_2 Nanomaterials and Their Application in Sonophotocatalytic Remediation of Treated Agro-Industrial Wastewater. *Materials (Basel).* **2021**, *14* (20), 6175.
(61) Paul, M.; Dhanasekar, M.; Bhat, S. V. Silver Doped H-MoO_3 Nanorods for Sonophotocatalytic Degradation of Organic Pollutants in Ambient Sunlight. *Appl. Surf. Sci.* **2017**, *418*, 113−118.
(62) Rajoriya, S.; Bargole, S.; George, S.; Saharan, V. K.; Gogate, P. R.; Pandit, A. B. Synthesis and Characterization of Samarium and

Nitrogen Doped TiO_2 Photocatalysts for Photo-Degradation of 4-Acetamidophenol in Combination with Hydrodynamic and Acoustic Cavitation. *Sep. Purif. Technol.* **2019**, *209*, 254−269.
(63) Ding, Z.; Sun, M.; Liu, W.; Sun, W.; Meng, X.; Zheng, Y. Ultrasonically Synthesized N-TiO_2/Ti_3C_2 Composites: Enhancing Sonophotocatalytic Activity for Pollutant Degradation and Nitrogen Fixation. *Sep. Purif. Technol.* **2021**, *276* (May), 119287.
(64) Kumawat, S.; Meghwal, K.; Kumar, S.; Ameta, R.; Ameta, C. Kinetics of Sonophotocatalytic Degradation of an Anionic Dye Nigrosine with Doped and Undoped Zinc Oxide. *Water Sci. Technol.* **2019**, *80* (8), 1466−1475.
(65) Hayati, F.; Khodabakhshi, M. R.; Isari, A. A.; Moradi, S.; Kakavandi, B. LED-Assisted Sonocatalysis of Sulfathiazole and Pharmaceutical Wastewater Using N, Fe Co-Doped TiO_2@SWCNT : Optimization, Performance and Reaction Mechanism Studies. *J. Water Process Eng.* **2020**, *38*, 101693.
(66) Jorfi, S.; Pourfadakari, S.; Kakavandi, B. A New Approach in Sono-Photocatalytic Degradation of Recalcitrant Textile Wastewater Using MgO@Zeolite Nanostructure under UVA Irradiation. *Chem. Eng. J.* **2018**, *343*, 95−107.
(67) Hu, G.; Yang, J.; Duan, X.; Farnood, R.; Yang, C.; Yang, J.; Liu, W.; Liu, Q. Recent Developments and Challenges in Zeolite-Based Composite Photocatalysts for Environmental Applications. *Chem. Eng. J.* **2021**, *417*, 129209.
(68) Chatti, R.; Rayalu, S. S.; Dubey, N.; Labhsetwar, N.; Devotta, S. Solar-Based Photoreduction of Methyl Orange Using Zeolite Supported Photocatalytic Materials. *Sol. Energy Mater. Sol. Cells* **2007**, *91* (2−3), 180−190.
(69) Jiang, N.; Shang, R.; Heijman, S. G. J.; Rietveld, L. C. High-Silica Zeolites for Adsorption of Organic Micro-Pollutants in Water Treatment : A Review. *Water Res.* **2018**, *144*, 145−161.
(70) Torkian, N.; Bahrami, A.; Hosseini-Abari, A.; Momeni, M. M.; Abdolkarimi-Mahabadi, M.; Bayat, A.; Hajipour, P.; Amini Rourani, H.; Abbasi, M. S.; Torkian, S.; Wen, Y.; Yazdan Mehr, M.; Hojjati-Najafabadi, A. Synthesis and Characterization of Ag-Ion-Exchanged Zeolite/TiO_2 Nanocomposites for Antibacterial Applications and Photocatalytic Degradation of Antibiotics. *Environ. Res.* **2022**, *207* (86), 112157.
(71) Isari, A. A.; Mehregan, M.; Mehregan, S.; Hayati, F.; Rezaei Kalantary, R.; Kakavandi, B. Sono-Photocatalytic Degradation of Tetracycline and Pharmaceutical Wastewater Using WO_3/CNT Heterojunction Nanocomposite under US and Visible Light Irradiations: A Novel Hybrid System. *J. Hazard. Mater.* **2020**, *390*, 122050.
(72) Xu, Q.; Zhang, L.; Cheng, B.; Fan, J.; Yu, J. Perspective S-Scheme Heterojunction Photocatalyst. *CHEMPR* **2020**, *6* (7), 1543−1559.
(73) Yuan, X.; Shen, D.; Zhang, Q.; Zou, H.; Liu, Z.; Peng, F. Z-Scheme Bi_2WO_6/$CuBi_2O_4$ Heterojunction Mediated by Interfacial Electric Field for Efficient Visible-Light Photocatalytic Degradation of Tetracycline. *Chem. Eng. J.* **2019**, *369* (March), 292−301.
(74) Aghaei, M.; Sajjadi, S.; Keihan, A. H. Sono-Coprecipitation Synthesis of ZnO/CuO Nanophotocatalyst for Removal of Parathion from Wastewater. *Environ. Sci. Pollut. Res.* **2020**, *27* (11), 11541−11553.
(75) Eshaq, G.; Wang, S.; Sun, H.; Sillanpää, M. Core/Shell $FeVO_4$@BiOCl Heterojunction as a Durable Heterogeneous Fenton Catalyst for the Efficient Sonophotocatalytic Degradation of p-Nitrophenol. *Sep. Purif. Technol.* **2020**, *231*, 115915.
(76) Guo, L.; Chen, Y.; Ren, Z.; Li, X.; Zhang, Q.; Wu, J.; Li, Y.; Liu, W.; Li, P.; Fu, Y.; Ma, J. Morphology Engineering of Type-II Heterojunction Nanoarrays for Improved Sonophotocatalytic Capability. *Ultrason. Sonochem.* **2021**, *81*, 105849.
(77) Zhang, W.; Mohamed, A. R.; Ong, W. Z-Scheme Photocatalytic Systems for Carbon Dioxide Reduction : Where Are We Now ? *Angewandte.* **2020**, *59*, 22894−22915.
(78) Zhou, P.; Yu, J.; Jaroniec, M. All-Solid-State Z-Scheme Photocatalytic Systems. *Adv. Mater.* **2014**, *26* (29), 4920−4935.
(79) Wu, F.; Li, X.; Liu, W.; Zhang, S. Highly Enhanced Photocatalytic Degradation of Methylene Blue over the Indirect All-Solid-State Z-Scheme g-C_3N_4-RGO-TiO_2 Nanoheterojunctions. *Appl. Surf. Sci.* **2017**, *405*, 60−70.
(80) Wang, S.; Zhu, B.; Liu, M.; Zhang, L.; Yu, J.; Zhou, M. Direct Z-Scheme ZnO/CdS Hierarchical Photocatalyst for Enhanced Photocatalytic H_2-Production Activity. *Appl. Catal., B* **2019**, *243*, 19−26.
(81) Qiao, J.; Zhang, H.; Li, G.; Li, S.; Qu, Z.; Zhang, M.; Wang, J.; Song, Y. Fabrication of a Novel Z-Scheme $SrTiO_3$/Ag_2S/$CoWO_4$ Composite and Its Application in Sonocatalytic Degradation of Tetracyclines. *Sep. Purif. Technol.* **2019**, *211*, 843−856.
(82) Low, J.; Jiang, C.; Cheng, B.; Wageh, S.; Al-Ghamdi, A. A.; Yu, J. A Review of Direct Z-Scheme Photocatalysts. *Small Methods* **2017**, *1* (5), 1700080.
(83) Babu, S. G.; Karthik, P.; John, M. C.; Lakhera, S. K.; Ashokkumar, M.; Khim, J.; Neppolian, B. Synergistic Effect of Sono-Photocatalytic Process for the Degradation of Organic Pollutants Using CuO-TiO_2/RGO. *Ultrason. Sonochem.* **2019**, *50*, 218−223.
(84) Pétrier, C.; Combet, E.; Mason, T. Oxygen-Induced Concurrent Ultrasonic Degradation of Volatile and Non-Volatile Aromatic Compounds. *Ultrason. Sonochem.* **2007**, *14* (2), 117−121.
(85) Dinesh, G. K.; Anandan, S.; Sivasankar, T. Synthesis of Fe-Doped Bi_2O_3 Nanocatalyst and Its Sonophotocatalytic Activity on Synthetic Dye and Real Textile Wastewater. *Environ. Sci. Pollut. Res.* **2016**, *23* (20), 20100−20110.
(86) Rahimi, S.; Ayati, B.; Rezaee, A. Optimization of Reaction Parameters for the Sonophotocatalytic Degradation of Hydroquinone. *Res. Chem. Intermed.* **2017**, *43* (3), 1935−1956.
(87) Yap, H. C.; Pang, Y. L.; Lim, S.; Lai, C. W.; Abdullah, A. Z. Enhanced Sonophotocatalytic Degradation of Paracetamol in the Presence of Fe-Doped TiO_2 Nanoparticles and H_2O_2. *Environ. Earth Sci.* **2020**, *79* (19), 457.
(88) Kohantorabi, M.; Moussavi, G.; Oulego, P.; Giannakis, S. Heterogeneous Catalytic Ozonation and Peroxone-Mediated Removal of Acetaminophen Using Natural and Modified Hematite-Rich Soil, as Efficient and Environmentally Friendly Catalysts. *Appl. Catal., B* **2022**, *301*, 120786.
(89) Gogate, P. R.; Pandit, A. B. Sonophotocatalytic Reactors for Wastewater Treatment: A Critical Review. *AIChE J.* **2004**, *50* (5), 1051−1079.
(90) Anipsitakis, G. P.; Dionysiou, D. D. Radical Generation by the Interaction of Transition Metals with Common Oxidants. *Environ. Sci. Technol.* **2004**, *38* (13), 3705−3712.
(91) Hayati, F.; Moradi, S.; Farshineh Saei, S.; Madani, Z.; Giannakis, S.; Isari, A. A.; Kakavandi, B. A Novel, Z-Scheme ZnO@AC@FeO Photocatalyst, Suitable for the Intensification of Photo-Mediated Peroxymonosulfate Activation: Performance, Reactivity and Bisphenol A Degradation Pathways. *J. Environ. Manage.* **2022**, *321* (July), 115851.
(92) Adewu-Yi, Y. G. Sonochemistry in Environmental Remediation. 2. Heterogeneous Sonophotocatalytic Oxidation Processes for the Treatment of Pollutants in Water. *Environ. Sci. Technol.* **2005**, *39* (22), 8557−8570.
(93) Chakma, S.; Praneeth, S.; Moholkar, V. S. Mechanistic Investigations in Sono-Hybrid (Ultrasound/Fe^{2+}/UVC) Techniques of Persulfate Activation for Degradation of Azorubine. *Ultrason. Sonochem.* **2017**, *38*, 652−663.
(94) Gogate, P. R. Treatment of Wastewater Streams Containing Phenolic Compounds Using Hybrid Techniques Based on Cavitation: A Review of the Current Status and the Way Forward. *Ultrason. Sonochem.* **2008**, *15* (1), 1−15.
(95) Ye, L.; Zhu, X.; Liu, Y. Numerical Study on Dual-Frequency Ultrasonic Enhancing Cavitation Effect Based on Bubble Dynamic Evolution. *Ultrason. Sonochem.* **2019**, *59* (July), 104744.
(96) Eshaq, G.; Wang, S.; Sun, H.; Sillanpaa, M. Superior Performance of $FeVO_4$@CeO_2 Uniform Core-Shell Nanostructures in Heterogeneous Fenton-Sonophotocatalytic Degradation of 4-Nitrophenol. *J. Hazard. Mater.* **2020**, *382*, 121059.

https://doi.org/10.1021/acsnanoscienceau.2c00058
ACS Nanosci. Au 2023, 3, 103−129

(97) Selvamani, P. S.; Vijaya, J. J.; Kennedy, L. J.; Mustafa, A.; Bououdina, M.; Sophia, P. J.; Ramalingam, R. J. Synergic Effect of Cu_2O/MoS_2/RGO for the Sonophotocatalytic Degradation of Tetracycline and Ciprofloxacin Antibiotics. *Ceram. Int.* **2021**, *47* (3), 4226−4237.
(98) Talukdar, K.; Saravanakumar, K.; Kim, Y.; Fayyaz, A.; Kim, G.; Yoon, Y.; Park, C. M. Rational Construction of CeO_2-ZrO_2@MoS_2 Hybrid Nanoflowers for Enhanced Sonophotocatalytic Degradation of Naproxen: Mechanisms and Degradation Pathways. *Composites, Part B* **2021**, *215*, 108780.
(99) Bolton, J. R.; Bircher, K. G.; Tumas, W.; Tolman, C. A. Figures-of-Merit for the Technical Development and Application of Advanced Oxidation Technologies for Both Electric- and Solar-Driven Systems. *Pure Appl. Chem.* **2001**, *73* (4), 627−637.
(100) Lin, C. C.; Lin, H. Y.; Hsu, L. J. Degradation of Ofloxacin Using UV/H_2O_2 Process in a Large Photoreactor. *Sep. Purif. Technol.* **2016**, *168*, 57−61.
(101) Yazdanbakhsh, A. R.; Eslami, A.; Massoudinejad, M.; Avazpour, M. Enhanced Degradation of Sulfamethoxazole Antibiotic from Aqueous Solution Using Mn-WO_3/LED Photocatalytic Process: Kinetic, Mechanism, Degradation Pathway and Toxicity Reduction. *Chem. Eng. J.* **2020**, *380*, 122497.
(102) Mohseni-Bandpei, A.; Eslami, A.; Rafiee, M.; Ghasemi, S. M.; Sadani, M.; Ghanbari, F. Heterogeneous Sonocatalytic Degradation of Atenolol Using $CuFe_2O_4$ from Aqueous Solution: Effects of Operational Parameters, Energy Consumption and Degradation Mechanism. *Int. J. Environ. Anal. Chem.* **2021**, *00* (00), 1−20.
(103) Bampos, G.; Frontistis, Z. Sonocatalytic Degradation of Butylparaben in Aqueous Phase over Pd/C Nanoparticles. *Environ. Sci. Pollut. Res.* **2019**, *26* (12), 11905−11919.
(104) Asgari, G.; Shabanloo, A.; Salari, M.; Eslami, F. Sonophotocatalytic Treatment of AB113 Dye and Real Textile Wastewater Using ZnO/Persulfate: Modeling by Response Surface Methodology and Artificial Neural Network. *Environ. Res.* **2020**, *184* (March), 109367.
(105) Mohamed, M. M.; Ghanem, M. A.; Khairy, M.; Naguib, E.; Alotaibi, N. H. Zinc Oxide Incorporated Carbon Nanotubes or Graphene Oxide Nanohybrids for Enhanced Sonophotocatalytic Degradation of Methylene Blue Dye. *Appl. Surf. Sci.* **2019**, *487* (April), 539−549.
(106) Khairy, M.; Naguib, E. M.; Mohamed, M. M. Enhancement of Photocatalytic and Sonophotocatalytic Degradation of 4-Nitrophenol by ZnO/Graphene Oxide and ZnO/Carbon Nanotube Nanocomposites. *J. Photochem. Photobiol., A* **2020**, *396*, 112507.
(107) Sunasee, S.; Wong, K. T.; Lee, G.; Pichiah, S.; Ibrahim, S.; Park, C.; Kim, N. C.; Yoon, Y.; Jang, M. Titanium Dioxide-Based Sonophotocatalytic Mineralization of Bisphenol A and Its Intermediates. *Environ. Sci. Pollut. Res.* **2017**, *24* (18), 15488−15499.
(108) ElMetwally, A. E.; Eshaq, G.; Al-Sabagh, A. M.; Yehia, F. Z.; Philip, C. A.; Moussa, N. A.; ElShafei, G. M. S. Insight into Heterogeneous Fenton-Sonophotocatalytic Degradation of Nitrobenzene Using Metal Oxychlorides. *Sep. Purif. Technol.* **2019**, *210*, 452−462.
(109) Benomara, A.; Guenfoud, F.; Mokhtari, M.; Boudjemaa, A. Sonolytic, Sonocatalytic and Sonophotocatalytic Degradation of a Methyl Violet 2B Using Iron-Based Catalyst. *React. Kinet. Mech. Catal.* **2021**, *132* (1), 513−528.
(110) Chong, M. N.; Jin, B.; Chow, C. W. K.; Saint, C. Recent Developments in Photocatalytic Water Treatment Technology: A Review. *Water Res.* **2010**, *44* (10), 2997−3027.
(111) Sun, J.; Rutherford, S. T.; Silhavy, T. J.; Huang, K. C. Physical Properties of the Bacterial Outer Membrane. *Nat. Rev. Microbiol.* **2022**, *20* (4), 236−248.
(112) Rojas, E. R.; Billings, G.; Odermatt, P. D.; Auer, G. K.; Zhu, L.; Miguel, A.; Chang, F.; Weibel, D. B.; Theriot, J. A.; Huang, K. C. The Outer Membrane Is an Essential Load-Bearing Element in Gram-Negative Bacteria. *Nature* **2018**, *559* (7715), 617−621.
(113) Yusof, N. S. M.; Babgi, B.; Alghamdi, Y.; Aksu, M.; Madhavan, J.; Ashokkumar, M. Physical and Chemical Effects of Acoustic Cavitation in Selected Ultrasonic Cleaning Applications. *Ultrason. Sonochem.* **2016**, *29*, 568−576.
(114) Joyce, E.; Al-Hashimi, A.; Mason, T. J. Assessing the Effect of Different Ultrasonic Frequencies on Bacterial Viability Using Flow Cytometry. *J. Appl. Microbiol.* **2011**, *110* (4), 862−870.
(115) Mitoraj, D.; Jańczyk, A.; Strus, M.; Kisch, H.; Stochel, G.; Heczko, P. B.; Macyk, W. Visible Light Inactivation of Bacteria and Fungi by Modified Titanium Dioxide. *Photochem. Photobiol. Sci.* **2007**, *6* (6), 642−648.
(116) Erkan, A.; Bakir, U.; Karakas, G. Photocatalytic Microbial Inactivation over Pd Doped SnO_2 and TiO_2 Thin Films. *J. Photochem. Photobiol. A Chem.* **2006**, *184* (3), 313−321.
(117) Benabbou, A. K.; Derriche, Z.; Felix, C.; Lejeune, P.; Guillard, C. Photocatalytic Inactivation of Escherischia Coli. Effect of Concentration of TiO_2 and Microorganism, Nature, and Intensity of UV Irradiation. *Appl. Catal. B Environ.* **2007**, *76* (3−4), 257−263.
(118) Habeeb Rahman, A. P.; Pranjal; Kumar Behera, S.; Mishra, A.; Stålsby Lundborg, C.; Tripathy, S. K. Transcriptomic Regulation of Salmonella Typhimurium during Sonophotocatalysis and the Effect of Stress Adaptation on the Antibiotic Resistance and Tolerance Post-Treatment. *Chem. Eng. J.* **2022**, *446* (P4), 137442.
(119) Sun, X.; Liu, J.; Ji, L.; Wang, G.; Zhao, S.; Yoon, J. Y.; Chen, S. A Review on Hydrodynamic Cavitation Disinfection: The Current State of Knowledge. *Sci. Total Environ.* **2020**, *737*, 139606.
(120) Mukherjee, A.; Das, S.; Ahn, Y. H. Sono-Photocatalytic Disinfection of High Strength Multi-Drug Resistant Klebsiella Pneumonia in Presence of Blue LED-Active CdS Nanorods. *J. Environ. Chem. Eng.* **2022**, *10* (8), 108460.
(121) Nithya, A.; Jeevakumari, H. L.; Rokesh, K.; Ruckmani, K.; Jeganathan, K.; Jothivenkatachalam, K. A Versatile Effect of Chitosan-Silver Nanocomposite for Surface Plasmonic Photocatalytic and Antibacterial Activity. *J. Photochem. Photobiol. B Biol.* **2015**, *153*, 412−422.
(122) Dalrymple, O. K.; Stefanakos, E.; Trotz, M. A.; Goswami, D. Y. A Review of the Mechanisms and Modeling of Photocatalytic Disinfection. *Appl. Catal. B Environ.* **2010**, *98* (1−2), 27−38.
(123) Rahman, A. P. H.; Dash, S.; Mohanty, P. S.; Mishra, A.; Lundborg, C. S.; Tripathy, S. K. Sonophotocatalytic Disinfection of Shigella Species under Visible Light Irradiation: Insights into Its Molecular Mechanism, Antibacterial Resistance and Biofilm Formation. *Environ. Res.* **2020**, *187*, 109620.
(124) Habeeb Rahman, A. P.; Misra, A. J.; Das, S.; Das, B.; Jayabalan, R.; Suar, M.; Mishra, A.; Tamhankar, A. J.; Lundborg, C. S.; Tripathy, S. K. Mechanistic Insight into the Disinfection of Salmonella Sp. by Sun-Light Assisted Sonophotocatalysis Using Doped ZnO Nanoparticles. *Chem. Eng. J.* **2018**, *336*, 476−488.
(125) Joy, J.; Mathew, J.; George, S. C. Nanomaterials for Photoelectrochemical Water Splitting - Review. *Int. J. Hydrogen Energy* **2018**, *43* (10), 4804−4817.
(126) Zhao, Y.; Zhang, S.; Shi, R.; Waterhouse, G. I. N.; Tang, J.; Zhang, T. Two-Dimensional Photocatalyst Design: A Critical Review of Recent Experimental and Computational Advances. *Mater. Today* **2020**, *34* (April), 78−91.
(127) Zhang, X.; Yuan, X.; Jiang, L.; Zhang, J.; Yu, H.; Wang, H.; Zeng, G. Powerful Combination of 2D g-C_3N_4 and 2D Nanomaterials for Photocatalysis: Recent Advances. *Chem. Eng. J.* **2020**, *390*, 124475.
(128) Ji, M.; Liu, Y.; Di, J.; Chen, R.; Chen, Z.; Xia, J.; Li, H. N-CQDs Accelerating Surface Charge Transfer of $Bi_4O_5I_2$ Hollow Nanotubes with Broad Spectrum Photocatalytic Activity. *Appl. Catal. B Environ.* **2018**, *237* (June), 1033−1043.
(129) Rodríguez-Seco, C.; Wang, Y. S.; Zaghib, K.; Ma, D. Photoactive Nanomaterials Enabled Integrated Photo-Rechargeable Batteries. *Nanophotonics* **2022**, *11* (8), 1443−1484.
(130) Chatterjee, S.; Bhattacharyya, K.; Ayyub, P.; Tyagi, A. K. Photocatalytic Properties of One-Dimensional Nanostructured Titanates. *J. Phys. Chem. C* **2010**, *114* (20), 9424−9430.
(131) Zhang, M.; Lu, M.; Lang, Z. L.; Liu, J.; Liu, M.; Chang, J. N.; Li, L. Y.; Shang, L. J.; Wang, M.; Li, S. L.; Lan, Y. Q. Semiconductor/Covalent-Organic-Framework Z-Scheme Heterojunctions for Artifi-

cial Photosynthesis. *Angew. Chemie - Int. Ed.* **2020**, *59* (16), 6500–6506.
(132) Villa, K.; Sopha, H.; Zelenka, J.; Motola, M.; Dekanovsky, L.; Beketova, D. C.; Macak, J. M.; Ruml, T.; Pumera, M. Enzyme-Photocatalyst Tandem Microrobot Powered by Urea for Escherichia Coli Biofilm Eradication. *Small* **2022**, *18* (36), 2106612.
(133) Ussia, M.; Urso, M.; Kment, S.; Fialova, T.; Klima, K.; Dolezelikova, K.; Pumera, M. Light-Propelled Nanorobots for Facial Titanium Implants Biofilms Removal. *Small* **2022**, *18* (22), 2200708.
(134) Moo, J. G. S.; Mayorga-Martinez, C. C.; Wang, H.; Teo, W. Z.; Tan, B. H.; Luong, T. D.; Gonzalez-Avila, S. R.; Ohl, C. D.; Pumera, M. Bjerknes Forces in Motion: Long-Range Translational Motion and Chiral Directionality Switching in Bubble-Propelled Micromotors via an Ultrasonic Pathway. *Adv. Funct. Mater.* **2018**, *28* (25), 1702618.
(135) Li, J.; Mayorga-Martinez, C. C.; Ohl, C. D.; Pumera, M. Ultrasonically Propelled Micro- and Nanorobots. *Adv. Funct. Mater.* **2022**, *32* (5), 2102265.

https://doi.org/10.1021/acsnanoscienceau.2c00058
ACS Nanosci. Au 2023, 3, 103–129